

1 Effect of clay content and distribution on hydraulic and geophysical properties of  
2 synthetic sand-clay mixtures

3  
4  
5  
6  
7 Gordon Osterman: Department of Earth and Environmental Science, Rutgers University-

8 Newark, Newark, NJ, USA; [gko4@rutgers.edu](mailto:gko4@rutgers.edu) (corresponding author)

9 Madhuri Sugand: Lancaster Environment Centre, Lancaster University, Lancaster, UK,

10 Currently at the REACH Centre, Lancaster University, Lancaster, UK;

11 [madhurisugand@outlook.com](mailto:madhurisugand@outlook.com)

12 Kristina Keating: Department of Earth and Environmental Science, Rutgers University-

13 Newark, Newark, NJ, USA; [kmkeat@newark.rutgers.edu](mailto:kmkeat@newark.rutgers.edu)

14 Andrew Binley: Lancaster Environment Centre, Lancaster University, Lancaster, UK;

15 [a.binley@lancaster.ac.uk](mailto:a.binley@lancaster.ac.uk)

16 Lee Slater: Department of Earth and Environmental Science, Rutgers University-Newark,

17 Newark, NJ, USA: [lslater@newark.rutgers.edu](mailto:lslater@newark.rutgers.edu)

18

19

## ABSTRACT

20 Geophysical methods show promise for detecting the spatial variability of subsurface  
21 clay content and its effect on subsurface hydraulic properties. We present a laboratory study that  
22 examines the influence of clay content and distribution on the relationships between hydraulic  
23 conductivity,  $K$ , and the physical and geophysical properties of the media. Two geophysical  
24 methods are investigated: spectral induced polarization (SIP) and nuclear magnetic resonance  
25 (NMR). We used synthetic sediment mixtures of sand and up to 10% kaolinite clay by mass; the

1 clay was homogeneously mixed or was present as large (~5 mm) clusters distributed through the  
2 sample.  $K$  varies moderately well (normalized root-mean square error,  $NRMSE = 0.393$ ) with the  
3 pore-volume normalized surface area,  $S_{por}$ , a proxy measure of clay content, in the homogeneous  
4 samples and poorly ( $NRMSE = 0.507$ ) when the clustered samples are included in the fit. SIP  
5 parameters show moderately good to excellent fits with  $S_{por}$  for homogeneous samples  
6 ( $NRMSE=0.0783$  to  $0.139$ ) and moderately good to good fits for clustered samples  
7 ( $NRMSE=0.140$  to  $0.336$ ) and the coefficients describing the polarizability of the samples depend  
8 on clay distribution. NMR parameters vary moderately well with  $S_{por}$  in the homogeneous  
9 samples ( $NMRSE=0.341$  to  $0.412$ ) and poorly ( $NMRSE=1.08$  to  $6.04$ ) in the clustered samples.  
10 SIP parameters vary moderately well with  $K$  ( $NRMSE=0.301$  to  $0.466$ ), however, the relationship  
11 between the SIP parameters and  $K$  is compromised by the non-negligible polarization of the clay  
12 clusters. NMR parameters show good to excellent fits with  $K$  ( $NRMSE=0.0789$  to  $0.116$ ). For  
13 both SIP and NMR, fitting homogeneous and clustered samples together does not compromise  
14 the fit quality. These results suggest that the geophysical measurements are better predictors of  $K$   
15 in heterogeneous porous media than bulk measures of pore geometry such as  $S_{por}$ .

## 16 INTRODUCTION

17 Accurate hydrogeological models require that the distribution of hydraulic properties in  
18 the system is well-quantified. Typically, the hydrogeology is characterized using aquifer tests  
19 performed in boreholes drilled into the groundwater system. In heterogeneous aquifers, a sparse  
20 network of wells may not accurately resolve the spatial variation in hydraulic properties. Of  
21 particular interest are the quantity and distribution of clay minerals throughout the subsurface,

1 which are known to have a disproportionate impact on subsurface hydraulic properties,  
2 particularly hydraulic conductivity (Neuzil, 1986; Keller et al., 1989).

3         Geophysical methods offer relatively fast and easy means of assessing spatial variations  
4 in the physical and hydraulic properties of the subsurface (see e.g. Binley et al., 2015) and have  
5 been used to map clay in the subsurface for decades (e.g. Palacky, 1987). Two relatively new  
6 methods in groundwater geophysics, spectral induced polarization (SIP) and nuclear magnetic  
7 resonance (NMR), are sensitive to the physical properties of porous media that control fluid flow  
8 (Weller et al., 2010; Minagawa et al., 2008), allowing researchers to develop petrophysical  
9 models using SIP and NMR parameters to estimate hydraulic conductivity (Börner et al., 1996;  
10 Revil et al., 2015; Seevers, 1966; Dlubac et al., 2013; Osterman et al., 2016). Furthermore,  
11 studies have shown that SIP and NMR signals are sensitive to variations in clay content (e.g.  
12 Vinegar and Waxman, 1984; Okay et al., 2014; Costabel and Yaramanci, 2013).

13         Clay distribution is known to control electrical measurements in synthetic sediments.  
14 Wildenschild et al. (2000) tested the effect of montmorillonite distribution on electrical  
15 conductivity measurements, hydraulic conductivity, and the hydraulic radius estimated using the  
16 approach of Revil and Cathles (1999). They found that surface conduction decreased when the  
17 clay was clustered as opposed to homogeneously distributed. Sugand (2015) extended the  
18 approach of Wildenschild et al. (2000) to study the impact of clay distribution on SIP  
19 measurements and SIP-hydraulic conductivity models. They found that while the SIP  
20 measurements were sensitive to the distribution of clay, the tested SIP-hydraulic conductivity  
21 models from the literature (Revil 2012; Weller et al., 2015a) performed well regardless of clay

1 distribution. However, their work did not include direct measurements of the pore geometry of  
2 their samples.

3         Previous studies have examined the effect clay heterogeneity on the NMR response of  
4 water-saturated sediments. Anand et al., (2006) found that increasing the kaolinite or bentonite  
5 content within homogeneous sand-clay mixtures resulted in a shift in the NMR relaxation time  
6 distribution to shorter relaxation times. However, increasing the clay content when distributed as  
7 a laminated surface within a sand matrix caused a second, short relaxation time peak to appear.  
8 In clay-bearing natural soils, Stingaciu et al. (2009) found that NMR relaxation time distributions  
9 compared well with pore size distributions measured from mercury injection and water retention  
10 curves. However, the authors found that the surface area normalized by pore volume did not  
11 correspond to the pore geometry detected by the NMR measurements. The effect of  
12 heterogeneous pore size distributions on NMR in unconsolidated materials has been studied in  
13 microporous silica beads (Hinedi et al. 1997) and in zeolites (Swanson et al., 2015). In both  
14 cases, the bimodal pore size distributions were reflected in the NMR relaxation time  
15 distributions. However, Hinedi et al. (1997) found that the surface area normalized by pore  
16 volume was dominantly controlled by the microporosity whereas the NMR measurements were  
17 more sensitive to the intergranular pores. While these previous studies have examined the effect  
18 of clay heterogeneity on the NMR response, they did not explore how the clay distribution  
19 impacted the link between the NMR parameters and the hydraulic properties of the sediments.

20         In this laboratory study, we extend the work of Wildenschild et al. (2000), Anand et al.  
21 (2006), and Sugand (2015) by posing the following research question: what are the impacts of  
22 clay content and clay distribution in synthetic sand-clay mixtures on the petrophysical links

1 between geophysical (SIP and NMR) parameters and the measured physical and hydraulic  
2 parameters? We mix clean, silica sand with up to 10% of kaolinite clay by mass and distribute  
3 the clay either homogeneously or as large (~5 mm in diameter), randomly dispersed clay  
4 clusters. The clay clusters are proxies for the heterogeneous clay distributions in natural  
5 sediments such as thin sand lenses; although they are imperfect reflections of natural sediments,  
6 they provide a strong contrast to compare homogenous clay distributions against. The results  
7 from this study represent a step towards understanding how the distribution of clay in  
8 unconsolidated sediments impacts measured geophysical parameters and petrophysical models.

9

10

## THEORY

### 11 **Hydraulic conductivity**

12 Hydraulic conductivity ( $K$ , units of m/s), is defined in Darcy's Law as the proportionality  
13 constant linking the rate of fluid flow to the hydraulic head gradient across a porous medium and  
14 quantifies the ability of a porous medium to conduct fluid flow. For unconsolidated samples,  $K$  is  
15 typically measured directly in the laboratory using one of two Darcy flow experiments: a  
16 constant head or a falling head experiment (Domenico and Schwartz, 1990). Alternatively,  $K$  can  
17 be estimated from characteristic physical properties of the porous medium; combining Darcy's  
18 Law with the Hagen-Poiseuille Law shows that  $K$  is proportional to the square of a characteristic  
19 pore size (Bear, 1972). Johnson et al. (1987) rigorously defined this length scale as the  
20 dynamically interconnected hydraulic radius, which we refer to simply as the hydraulic radius.

1 However, it is difficult to measure the hydraulic radius directly, especially in unconsolidated  
 2 sediments, so researchers have explored using proxy measures of hydraulic radius to estimate  $K$ .

3 An alternate pore geometry used for estimating hydraulic conductivity is the pore-volume  
 4 normalized surface area ( $S_{por}$ , units of  $1/\mu\text{m}$ ), which is often considered to be inversely  
 5 proportional to the hydraulic radius.  $S_{por}$  can be calculated from,

$$S_{por} = S_{SA} \rho_g \frac{1-\phi}{\phi}, \quad (1)$$

6 where  $S_{SA}$  is the specific surface area ( $\text{m}^2/\text{g}$ ),  $\phi$  is the porosity (-), and  $\rho_g$  is the matrix density  
 7 ( $\text{g}/\text{m}^3$ ). Clay has a much higher  $S_{SA}$  than sand and in unconsolidated sand-clay mixtures with a  
 8 single type of sand and clay  $S_{por}$  is a rough proxy for the clay content with high  $S_{por}$  values  
 9 indicating high clay content.

10 Estimating  $K$  from  $S_{por}$  can be done using the Kozeny-Carman capillary bundle model of  
 11 the form (Carman, 1939),

$$K = A_{KC} \phi S_{por}^{-2}, \quad (2)$$

12 where  $A_{KC}$  is a fitting coefficient that accounts for the tortuosity of the pore space and varies  
 13 based on the soil texture (Chapuis and Aubertin, 2003). Ozgumus et al. (2014) compiled a set of  
 14  $A_{KC}$  values from numerous computational and experimental studies ranging between  $4-14 \times 10^{-5}$   
 15  $\text{m}/\mu\text{m}^2/\text{s}$ . Although the exponent in equation 2 is typically set to 2 (Carrier, 2003), other  
 16 researchers have suggested alternative values. For instance, Pape et al. (1987) suggest a value of  
 17 3.1 based on a fractal model of the pore space.

1           The dependence of  $K$  on  $S_{por}$  in equation 2 suggests that increasing the clay content of a  
 2 porous medium will reduce  $K$ . Chapuis and Aubertin (2003) cautioned that equation 2 only holds  
 3 for clayey sediments when they are fully saturated and non-compacted. Furthermore,  $S_{por}$  is a  
 4 bulk property of a porous medium and equation 2 implicitly assumes that  $S_{por}$  is homogeneous  
 5 throughout the volume of interest. In heterogeneous sediments, equation 2 may not be valid.

6

### 7 **Spectral induced polarization**

8           SIP, which evolved from the use of induced polarization in mineral exploration, is  
 9 employed for a wide range of near-surface geophysical problems, including hydraulic parameter  
 10 estimation. In this section we briefly review the theory of SIP; more thorough presentations can  
 11 be found in: Vinegar and Waxman (1984); Revil and Florsch (2010); Weller et al. (2010);  
 12 Kemna et al. (2012); Revil (2012, 2013); Revil et al. (2017); and Weller et al. (2015a). The SIP  
 13 measurement involves injecting a sinusoidal alternating electrical current into a porous medium  
 14 at low frequencies (mHz to kHz) and measuring the resulting phase-delayed sinusoidal voltage.  
 15 The measured complex electrical conductivity  $\sigma^*$  (S/m) can be decomposed into real ( $\sigma'$ ) and  
 16 quadrature ( $\sigma''$ ) components,

$$\sigma^*(f) = |\sigma| e^{i\theta(f)} = \sigma'(f) + i\sigma''(f), \quad (3)$$

$$\tan(\theta) = \frac{\sigma''(f)}{\sigma'(f)}, \quad (4)$$

17 where  $|\sigma|$  is the magnitude of the complex conductivity,  $\theta$  is the phase angle (rad),  $f$  is the  
 18 injected current frequency (Hz), and  $i$  is the unit imaginary number.

1           The  $\sigma'$  component quantifies electrolytic conduction resulting from the unrestricted  
 2 electromigration of ions through both the pore fluid and the electrical double layer (EDL) that  
 3 forms at the fluid-mineral interface (Sen et al., 1988; Revil and Cathles, 1999),

$$\sigma'(f) = \frac{1}{F} \sigma_f + \sigma'_s. \quad (5)$$

4  $F$  is Archie's electrical formation factor (Archie, 1942; Vinegar and Waxman, 1984) which is  
 5 related to the tortuosity-normalized porosity,  $\sigma_f$  is the saturating fluid conductivity, and  $\sigma'_s$  is the  
 6 in-phase surface conductivity at the pore interface. While  $F$  and  $\sigma'_s$  are functions of the pore  
 7 geometry (Weller et al., 2013, Revil 2013), the parameters cannot be readily disentangled from  
 8  $\sigma_f$ , which makes  $\sigma'$  a non-ideal parameter for petrophysical relationships (Slater, 2007). The  $\sigma''$   
 9 component represents restricted electromigration, which results in a reversible build-up of ions,  
 10 or polarization, throughout the pore space. In saturated geological media composed of insulating  
 11 grains, ionic polarization is thought to be caused by two dominant mechanisms in the 0.01-100  
 12 Hz range: EDL polarization (Leroy et al., 2008; Revil, 2012; Revil, 2013, Revil et al., 2017) and  
 13 membrane polarization (Marshall and Madden, 1959; Titov et al., 2002). Both mechanisms are  
 14 strongly dependent on grain and pore geometry (Revil and Florsch, 2010; Bückner and Hördt,  
 15 2013) and relatively insensitive to  $\sigma_f$  (Weller et al., 2011).

16           A single, characteristic value of  $\sigma''$  is often used to represent an entire SIP spectrum and  
 17  $\sigma''$  at 1 Hz ( $\sigma''_{1Hz}$ ) is commonly chosen as it is a frequency readily measurable using laboratory,  
 18 borehole, and field SIP equipment. Weller et al. (2010) compiled SIP data on homogeneously  
 19 mixed sand and sand-clay sediments from Slater and Glaser (2003) and Slater et al. (2006),  
 20 which showed an approximately linear relationship between  $\sigma''_{1Hz}$  and  $S_{por}$ . Revil et al. (2017)



1 extend on this relationship and developed a model of electrical conduction in soils where  $\sigma''_{1Hz}$  is  
 2 approximated by  $S_{por}$  as,

$$\sigma''_{1Hz} = C_s \frac{S_{por}}{F(1-\phi)}. \quad (6)$$

3 Here  $C_s = 7.36 \times 10^{-2}$  mS um/m per Revil et al. (2013; 2017) (see derivation in Appendix A).  
 4 Similar to the specific polarizability from Weller et al. (2010),  $C_s$  is a function of ionic density  
 5 and mobility in the Stern Layer at the fluid-mineral interface and therefore a second-order  
 6 function of pore fluid chemistry (Weller et al., 2011). However, the specific polarizability as  
 7 defined by Weller et al. (2010) is a proportionality constant between  $S_{por}$  and  $\sigma''$  which,  
 8 according to equation 6, suggests that the specific polarizability implicitly contains information  
 9 on  $F$  and  $\phi$  whereas  $C_s$  is independent of these parameters. Note that the units given for  $C_s$   
 10 simplify to (nS) but are reported as (mS um/m) to reflect the units of the measurements used to  
 11 derive  $C_s$ .

12 Petrophysical information may be extracted from the entire SIP spectrum by modeling it  
 13 with a phenomenological relaxation time model such as a Debye-decomposition (Nordsiek and  
 14 Weller, 2008; Zisser et al., 2010). In the Debye-decomposition approach to modeling SIP spectra  
 15 of Nordsiek and Weller (2008),  $\sigma^*(f)$  is given by a superposition of  $N$  Debye models,

$$\sigma^*(f) = \sigma_0 \left( 1 - \sum_{j=1}^N m_j \left( 1 - \frac{1}{1 + i2\pi f \tau_j} \right) \right)^{-1}, \quad (7)$$

$$\sum_{j=1}^N m_j = m_t = \frac{\sigma_\infty - \sigma_0}{\sigma_\infty}, \quad (8)$$

1 where  $m_j$  (unitless) and  $\tau_j$  (s) are the chargeability and the SIP relaxation time parameters for the  
 2  $j^{\text{th}}$  relaxation term,  $m_t$  is the total chargeability of the pore space (Sumner, 1976),  $\sigma_\infty$  is the  
 3 conductivity magnitude at the high frequency asymptote and  $\sigma_0$  is the conductivity magnitude at  
 4 zero frequency.  $m_t$  defines the relative change in the magnitude of  $\sigma^*$  over the frequency  
 5 spectrum. The normalized chargeability ( $m_n$ , units of S/m) is calculated by scaling  $m_t$  by  $\sigma_0$ ,

$$m_n = m_t \sigma_0. \quad (9)$$

6 Weller et al. (2010) found that  $m_n$  varies linearly with  $S_{por}$ , and Revil et al. (2017) gave the  
 7 following expression,

$$m_n = C_m \frac{S_{por}}{F(1-\phi)}, \quad (10)$$

8 where  $C_m$  is similar to  $C_s$  and the specific polarizability (Weller et al., 2010). From Revil et al.  
 9 (2013; 2017),  $C_m = 5.96 \times 10^{-1}$  mS um/m (see Appendix A).

10  $K$  can be estimated from SIP parameters based on power-law relationships,

$$K = \frac{A_s}{F(\sigma''_{1Hz})^2}. \quad (11)$$

$$K = \frac{A_m}{Fm_n^2}. \quad (12)$$

11 Where  $A_s$  and  $A_p$  are fitting coefficients (mS<sup>2</sup>/m/s). Equations 11 and 12 are simplified versions  
 12 of the equations in Weller et al. (2015a), which were derived from 22 samples of unconsolidated  
 13 sediments. In the version of equation 11 given in Weller et al., (2015a) the exponent for  $\sigma''_{1Hz}$  is –  
 14 2.27, the exponent for  $F$  is –1.12, and  $A_s = 1.19 \times 10^{-6}$  mS<sup>2</sup>/m/s; in the version of equation 12

1 given in Weller et al. (2015a) the exponent for  $m_n$  is -2.21, the exponent for  $F$  is -1.07, and  $A_m$   
 2  $=9.55 \times 10^{-5}$  mS<sup>2</sup>/m/s. Note that these values of  $A_s$  and  $A_m$  were originally defined for permeability  
 3 ( $k$ ) models where permeability was measured in units of m<sup>2</sup>. For water-saturated media at 25°C,  
 4  $K=V*k$ , where  $V=1.10 \times 10^7$  m\*s and has been used to scale the coefficients in Weller et al.  
 5 (2015a) for use here. Although the models we use are not exactly the same as those from Weller  
 6 et al. (2015a), the exponents are sufficiently similar that we can compare our results to theirs.

7

## 8 **Nuclear magnetic resonance**

9 Geophysical applications of NMR focus on the detection of hydrogen protons in pore  
 10 fluids, primarily in water and hydrocarbons, to assess their quantity and mobility. A thorough  
 11 review of proton NMR for geophysical applications and hydraulic parameter estimation is  
 12 provided in: Timur (1969); Banavar and Schwartz (1987); Morriss et al. (1997); Kleinberg and  
 13 Horsfield (1990); Howard and Kenyon (1992); Kenyon et al. (1995); Kleinberg (1996);  
 14 Godefroy et al. (2001); and Behroozmand et al. (2015). The NMR experiment consists of tipping  
 15 the nuclear spins of the protons away from their equilibrium orientation with a static magnetic  
 16 field using a secondary oscillating magnetic field. After terminating the secondary magnetic  
 17 field, the protons relax back to their equilibrium orientation, a process that produces a  
 18 measurable signal,  $A(t)$  that can be modeled as a superposition of  $M$  exponential decays,

$$A(t) = A_0 \sum_{j=1}^M h_j e^{-t/T_{2j}}, \quad (13)$$

1 where  $A_0$  (arbitrary units) is the signal magnitude at time  $t=0$ ;  $h_j$  (-) and  $T_{2j}$  (s) are the signal  
 2 fraction and transverse relaxation time of the  $j^{\text{th}}$  portion of the signal, respectively. The  $A_0$  is  
 3 proportional to the number of protons in the pore space tipped into the transverse plane and thus  
 4 gives the water content in the pore space.

5 The measured  $T_2$  relaxation times arise from three parallel relaxation mechanisms,

$$T_2^{-1} = T_{2B}^{-1} + T_{2S}^{-1} + T_{2D}^{-1}, \quad (14)$$

6 where  $T_{2B}$  is the bulk relaxation time, which corresponds to relaxation occurring due to dipolar  
 7 spin-coupling between water molecules,  $T_{2S}$  is the surface relaxation time, which corresponds to  
 8 relaxation occurring due to proton-electron spin coupling at paramagnetic mineral sites at the  
 9 fluid-mineral interface, and  $T_{2D}$  is the diffusion relaxation time, which quantifies the apparent  
 10 relaxation that results from the dephasing of protons as they diffuse through pore-scale magnetic  
 11 field inhomogeneities. As  $T_{2B}$  and  $T_{2D}$  contain little information concerning the pore geometries  
 12 controlling fluid flow, it is desirable to minimize or eliminate their influence.  $T_{2B}$  has a constant  
 13 value for water ( $\sim 3$  s) that is much slower than  $T_{2S}$  and can be subtracted with little impact on  $T_2$   
 14 (e.g. Keating and Knight, 2007). The effect of  $T_{2D}$  can be mitigated by using a Carr-Purcell-  
 15 Meiboom-Gill, or CPMG (Meiboom and Gill, 1958) pulse sequence to rephase the proton spins  
 16 with very short pulse intervals, or echo times (Kleinberg and Horsfield, 1990; Anand and  
 17 Hirasaki, 2008).

18 Brownstein and Tarr (1979) found that  $T_{2S}$  is controlled by the distance a proton travels  
 19 before interacting with a pore wall, which is related to the size of the pore, as well as the density  
 20 and distribution of paramagnetic impurities at the surface quantified by the surface relaxivity,  $\rho_2$

1 ( $\mu\text{m/s}$ ) (Kleinberg, 1996). If relaxation occurs in the fast diffusion regime then each pore is  
 2 characterized by a single relaxation time  $T_{2j}$  and signal amplitude  $h_j$  (Brownstein and Tarr, 1979;  
 3 Kleinberg and Horsfield, 1990). Assuming  $\rho_2$  does not vary to a large degree within the observed  
 4 geological media (Foley et al., 1996), the distribution of  $T_2$  relaxation times in equation 13 may  
 5 be interpreted as a proxy for the pore size distribution of a system (Kleinberg, 1996), although in  
 6 certain geological environments (e.g. formations containing iron(III)-bearing minerals) this  
 7 assumption may not be true (Keating and Knight, 2012).

8 In relatively homogeneous porous media, the entire system may be characterized by a  
 9 single, characteristic relaxation rate  $T_{2S}^{-1}$ , where,

$$T_{2S}^{-1} = \rho_2 S_{por}. \quad (15)$$

10 The most commonly used characteristic value from the  $T_2$  distribution is the mean-log relaxation  
 11 time  $T_{2ml}$  as it incorporates information from the entire  $T_2$  distribution. We refer to surface  
 12 relaxivities derived using  $T_{2ml}$  as  $\rho_{2ml}$ . The relaxation time at the peak of the distribution,  $T_{2p}$ , has  
 13 also been shown to correlate well with the hydraulic radius (Keating, 2014; Osterman et al.,  
 14 2016) and to be well suited for estimating  $K$  (Dlugosch et al., 2013). Here we refer to surface  
 15 relaxivities derived using  $T_{2p}$  as  $\rho_{2p}$ . Godefroy et al. (2001) found for a set of clean silicon  
 16 carbide samples that  $\rho_2$  ranged from  $3 \leq \rho_2 \leq 5 \mu\text{m/s}$ . Similarly, Kleinberg (1996) found that  $\rho_2 = 3$   
 17  $\mu\text{m/s}$  for quartz. Note that the derived value of  $\rho_2$  depends on the characteristic  $T_2$  value and how  
 18 the pore geometry is measured. For example, Stingaciu et al. (2009) found that  $S_{por}$  was not a  
 19 good pore geometry to use for estimating  $\rho_2$  in natural, clay-bearing soils, as it did not reflect the  
 20 pore space heterogeneity in their samples.

1           In regularized inversions commonly used to extract the relaxation time distribution from  
 2 NMR data, the choice of regularization parameter can strongly impact the shape of the  $T_2$   
 3 distribution and the location of peaks.  $T_{2ml}$  is relatively robust to variations in the regularization  
 4 parameter, which makes it an appealing relaxation time to use. By contrast,  $T_{2p}$  may vary to a far  
 5 greater degree as a function of the regularization parameter and caution must be exercised when  
 6 interpreting  $T_{2p}$ .

7           Based on equation 15,  $K$  models such as the Schlumberger-Doll Research equation  
 8 (SDR) have been derived for NMR measurements (Seevers, 1966; Banavar and Schwartz, 1987)  
 9 with the form,

$$K = B_{m//p} \phi_{NMR}^n T_2^2, \quad (16)$$

10 where  $\phi_{NMR}$  is porosity estimated from the NMR signal amplitude  $A_0$ ,  $B_{m//p}$  refers to the fitting  
 11 coefficient where the subscript corresponds to the characteristic relaxation time used ( $ml$  for  $T_{2ml}$ ,  
 12 or  $p$  for  $T_{2p}$ ), and  $n$  is an exponent used to describe the tortuosity of the pore space. In the NMR  
 13 literature  $n$  is typically set to 4 (Kenyon et al., 1995). Maurer and Knight (2016) found that for a  
 14 broad range of borehole measurements in unconsolidated sedimentary environments,  $B_{ml} = 0.80$ –  
 15  $4.70 \text{ m/s}^3$  when  $n=4$ . Another model that is commonly used to estimate  $K$  is the Timur-Coates  
 16 (TC); the TC model is an empirical model that uses an estimate of the irreducible water volume,  
 17 determined from the NMR relaxation time distribution, to predict  $K$  (Timur, 1969; Coates et al.,  
 18 1991). Other researchers have developed models for  $K$  or  $k$  that are optimized for specific  
 19 geologic materials, such as unconsolidated coarse grain materials (Dlugosch et al., 2013), fine  
 20 grain sediments (Daigle and Dugan, 2009), and fine-grain clay rich mudstones (Daigle and  
 21 Dugan, 2011).

1

2

## MATERIALS AND METHODS

3

4

5

6

7

8

9

10

To test the effect of clay content and distribution in synthetic sand-clay mixtures on the relationships between the measured physical and hydraulic parameters and the geophysical parameters, we prepared 21 synthetic mixtures with varying ratios of sand and clay and collected  $S_{por}$ ,  $K$ , SIP, and NMR data on each sample. All measurements were run in 9.3 cm tall by 2.3 cm diameter cylindrical acrylic sample holders specially designed to support  $K$ , SIP and NMR measurements without disturbing or repacking the samples (see Wallace, 2015). The sand-clay mass ratios of 100-0, 99-1, 95-5, and 90-10 were used. For each clay concentration, three replicate samples were mixed to test the repeatability of the packing and saturation procedure.

11

### Sample preparation

12

13

14

15

16

Measurements were conducted on mixtures of Wedron silica sand (Wedron Silica Co.) and kaolinite clay (Fisher Scientific). The Wedron sand is a medium, well sorted, round, clean sand with a narrow grain size distribution centered at 300  $\mu\text{m}$  and a specific surface area  $S_{SA}=0.0388\pm 0.0001 \text{ m}^2/\text{g}$ . The kaolinite is a non-swelling, 1:1 phyllosilicate mineral with  $S_{SA}=11.552 \pm 0.0179 \text{ m}^2/\text{g}$ .

17

18

19

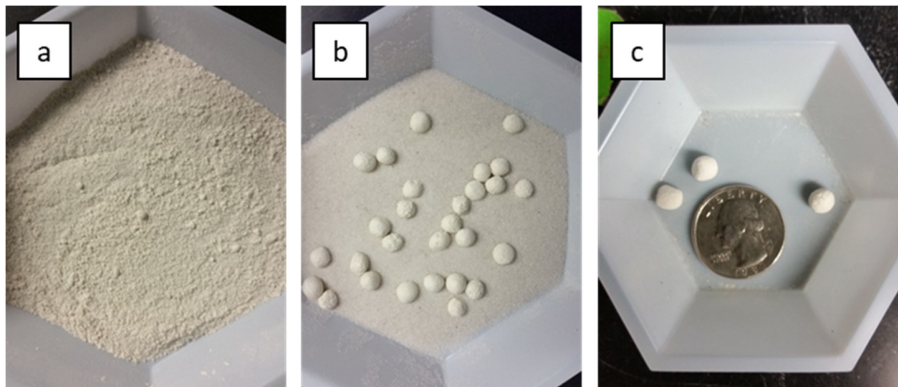
20

21

Homogeneous samples were packed by first drying the sand and clay, then mixing according to the following ratios: 100%, 99%, 95%, and 90% sand, by mass. Figure 1 shows examples of the homogeneous and clustered samples with 10% clay prior to packing. The mixed sediments were dry-packed into the sample holders, with care taken to ensure no clay layers formed. Clay clusters were created by dampening the clay with deionized water and then

1 forming it into ~5 mm diameter balls (Figure 1c) which were oven dried overnight, separate from  
2 the sand. To create the clustered samples, dry sand and clay clusters were alternately added to the  
3 sample holder to ensure the ratio of sand to clay was precisely known. The same sand-to-clay  
4 ratios were used for the clustered samples as the homogeneous samples. Care was taken to  
5 ensure that the clay clusters were not in contact with each other.

6 The following naming convention was used for all samples: The first letter refers to the  
7 sample type (H indicates homogeneously mixed and C indicates clay clusters), the following  
8 number indicates the percentage of clay (00, 01, 05, or 10), and the final letter indicates which  
9 repeat the sample is (A, B or C). For example, sample H01B refers to the second repeat of the  
10 homogeneous 1% clay samples.



11  
12 Figure 1: Examples of dry samples prior to packing, (a) 90% sand mixed homogeneously with  
13 10% clay; (b) 90% sand mixed with 10% clay clustered in ~5 mm balls; (c) clay clusters shown  
14 with a US quarter for scale.

15 All samples were vacuum saturated by pulling a strong vacuum on the dry samples before  
16 flooding the sample holder with a degassed 10 mM sodium chloride brine (corresponding to a  
17 fluid conductivity of  $0.11 \pm 0.01$  S/m at  $25^\circ\text{C}$ ). Electrolyte species and concentration were chosen  
18 to allow us to compare our results to other studies in the literature (e.g. Weller et al., 2010). Fluid



1 conductivities were determined by repeatedly measuring the outflow conductivity and waiting  
2 for the fluid conductivity to stabilize. Full saturation was confirmed by comparing the known  
3 sample volume to the estimated sample volume calculated from the mass of the saturating fluid  
4 and solid matrix, using densities of  $1.00 \text{ g/m}^3$ ,  $2.65 \text{ g/m}^3$ , and  $2.6 \text{ g/m}^3$  for the saturating fluid,  
5 sand, and kaolinite.

## 6 **Measurement methodologies**

7 A constant head approach was used to measure hydraulic conductivity (see Domenico  
8 and Schwartz, 1990) and  $K$  was estimated from the average of four inflow-outflow head  
9 differentials. A Micromeritics ASAP 2020 surface area analyzer was used to measure  $S_{SA}$  using  
10 the Brunauer, Emmitt, and Teller, or BET, method of gas adsorption porosimetry (Brunauer et  
11 al., 1938). We used krypton as the adsorbate due to the very low surface area of the Wedron  
12 sand. Measured  $S_{SA}$  was converted to  $S_{por}$  using the porosity calculated from the mass difference  
13 between saturated and dry columns normalized by the sample volume. Although BET  
14 measurements can underestimate the surface area in clays with large inter-granular surface area  
15 (see e.g. Weller et al., 2015b), kaolinite is a 1:1 clay with limited inter-granular surface area and  
16 so BET is an acceptable method for measuring  $S_{SA}$  for the samples used in this study.

17 Samples for BET analysis were prepared in two ways. Homogenous samples were dried  
18 and subsampled from their columns and packed into the BET sample holders. Subsampling was  
19 not an appropriate technique for the clustered samples, so we instead recreated clustered samples  
20 specifically for BET analysis according to the exact sand-clay ratio in the sample holder.

1 SIP samples were run on an Ontash and Ermac PSIP instrument (Ntarlagiannis and  
2 Slater, 2014) in the frequency range from 10 mHz to 1 kHz with 5 logarithmically spaced  
3 measurements per decade. Each measurement was replicated three times to ensure repeatability.  
4 The instrument was capable of resolving phase angles as low as 0.1 mrad. In one pure sand  
5 sample and three clustered clay samples, we observed low polarization in the 0.1–10 Hz  
6 frequency range that resulted in phase angles smaller than 0.1 mrad; measurements at these  
7 frequencies were excluded from analysis. For ease of comparison with literature results, we use  
8  $\sigma''_{1Hz}$  as the characteristic SIP polarization magnitude parameter. To calculate  $m_n$ , we calculated  
9  $m_r$ -distributions and  $\sigma_0$  using the Monte-Carlo Markov Chain approach of Keery et al. (2012)  
10 where random walk simulations sample a probability distribution of possible solutions.

11 Electrical measurements were conducted with a range of saturating fluid conductivities in  
12 order to accurately measure  $F$  (Vinegar and Waxman, 1984; Weller et al. 2013; Revil et al.,  
13 2015). All SIP parameters are calculated from measurements at low salinity, corresponding to  $\sigma_f$   
14 values of approximately 0.11 S/m. For the homogeneous clay samples, high-salinity  
15 measurements were unavailable for the samples presented here. However, electrical  
16 measurements were conducted over a range of salinities corresponding to  $\sigma_f$  values ranging from  
17 approximately 0.11 S/m to 10 S/m on an alternate set of sand-clay mixtures packed using the  
18 same methodology, materials, and sand-clay ratios. A comparison of the  $S_{por}$ , SIP and NMR data  
19 between the data presented here and the alternate data set shows a high degree of repeatability.  
20 For each sand-clay ratio, we assign an average value of  $F$  from the same sand-clay ratio from the  
21 alternate data set. For the clustered clay samples, electrical measurements were made at two  
22 salinities (approximately 0.11 S/m and 5 S/m) and these measurements were used to calculate  $F$ .

1 All NMR data were collected using a 2.0 MHz Magritek Rock Core Analyzer. The  
2 CPMG pulse sequence was used with echo times of 200, 400, 800, and 1600  $\mu\text{s}$ , a total  
3 measurement time of 10 s, and a recovery time of 10 s. Three cycles of 16 stacks were collected  
4 at each echo time to assess measurement repeatability. Measurements from the samples were  
5 compared using the 200  $\mu\text{s}$  echo time data; longer echo times were used to assess the influence of  
6  $T_{2D}$ . Data were inverted using a non-negative least squares algorithm with second-order  
7 Tikhonov regularization, producing a log-spaced  $T_2$  distribution from 100  $\mu\text{s}$  to 10 s (Whittall et  
8 al., 1991). The inversion regularization parameter was selected using the approach of Costabel  
9 and Yaramanci (2013) to produce the simplest model that minimizes the data misfit. Using this  
10 approach, the same regularization parameter was selected for all samples, allowing us to ignore  
11 the impact of regularization on  $T_{2p}$ .  $T_{2B}$  was determined from an average of measurements on  
12 three samples of 10 mM sodium chloride brine and found to be 2.9 s.

13 Characteristic  $T_2$ -relaxation times  $T_{2ml}$  and  $T_{2p}$  were used for the petrophysical analysis.  
14 To calculate  $T_{2ml}$ , we first eliminated any portion of the  $T_2$  distribution associated with standing  
15 water in the columns, as signal associated with this water is insensitive to the hydraulic  
16 properties of the sand-clay mixtures. The effect of bulk relaxation was removed by subtracting  
17  $T_{2B}$  from  $T_{2ml}$  and  $T_{2p}$ . Following the procedure of Keating and Knight (2007), we fit a linear  
18 regression between the square of the echo time and inverse relaxation time to demonstrate the  
19 negligible impact of  $T_{2D}$  at an echo time of 200  $\mu\text{s}$ . To ensure that relaxation occurred within the  
20 fast diffusion regime, we calculated  $\rho_2$  from equation 15 to assess whether the samples met the  
21 fast diffusion criteria,  $\rho_2 R/D < 0.1$ , where  $R$  ( $\mu\text{m}$ ) is the average distance a proton travels during  
22 relaxation and  $D$  ( $\mu\text{m}^2/\text{s}$ ) is the self-diffusion coefficient of water (Brownstein and Tarr, 1979;  
23 Ryu, 2009).

1

2 **Fitting coefficients and statistics**

3 The fitting coefficients ( $A_{KC}$  for equation 2,  $C_s$  for equation 6,  $C_m$  for equation 10,  $A_s$  for  
 4 equation 11,  $A_m$  for equation 12,  $\rho_2$  for equation 15, and  $B_{ml}$  and  $B_p$  for equation 16) were  
 5 calculated as the mean-difference between log-transformed independent and dependent  
 6 parameters,

$$coef = \exp\left(\frac{1}{N} \sum_{j=1}^N (\log \hat{y}_j - \log y_j)\right), \quad (17)$$

7 where  $coef$  refers to the fitting coefficient,  $N$  is the number of data points,  $\hat{y}_j$  is the  $j^{th}$  dependent  
 8 variable, and  $y_j$  is the  $j^{th}$  independent variable, which we set equal to the left-hand side of the  
 9 relevant petrophysical equation or  $K$  model. To measure the quality of the fit, we calculate the  
 10 normalized root mean square error ( $NRMSE$ ) from,

$$NRMSE = \frac{1}{\log_{10} \hat{y}_{max} - \log_{10} \hat{y}_{min}} \sqrt{\frac{1}{N} \sum_{j=1}^N (\log_{10} \hat{y}_j - \log_{10} y_j)^2}, \quad (18)$$

11 where  $\hat{y}_{max}$  is the maximum predicted value and  $\hat{y}_{min}$  is the minimum predicted value. Since the  
 12  $NRMSE$  normalizes for both the number of samples as well as the data range, we can compare  
 13 values of  $NRMSE$  between datasets. To assess the quality of the fits determined using equation  
 14 17, we use the following criteria:  $NRMSE < 0.1$  correspond to excellent fits,  $0.1 < NRMSE < 0.3$ ,  
 15 correspond to good fits,  $0.3 < NRMSE < 0.5$  correspond to moderately good fits, while  $NRMSE > 0.5$   
 16 correspond to poor fits.

1

2

## RESULTS

3

4

5

6

7

8

9

All values of  $K$ ,  $S_{por}$ ,  $\phi$ ,  $F$ , characteristic SIP parameters ( $\sigma''_{1Hz}$  and  $m_n$ ), and characteristic NMR parameters used in this study are reported in Table 1.  $K$  varies from  $4.98 \times 10^{-6}$  m/s to  $2.74 \times 10^{-4}$  m/s in the homogeneous samples, but only from  $1.52 \times 10^{-4}$  m/s to  $2.83 \times 10^{-4}$  m/s in the clustered samples.  $S_{por}$  varies from 0.14  $1/\mu\text{m}$  to 6.26  $1/\mu\text{m}$  in the homogeneous samples and from 0.63  $1/\mu\text{m}$  to 5.68  $1/\mu\text{m}$  in the clustered samples. For all samples,  $\phi$  varies from 0.36 to 0.40 with a mean of 0.38, and  $F$  varies from 4.10 to 6.26. No trend in  $\phi$  or  $F$  is observed with increasing clay content which is likely a result of the low clay contents investigated.

10

11

12

13

14

15

Table 1: List of physical and geophysical parameters used for this study. Physical parameters include the hydraulic conductivity ( $K$ ), the gravimetric porosity ( $\phi$ ), the pore volume normalized surface area ( $S_{por}$ ), and the electrical formation factor ( $F$ ). The geophysical parameters include the SIP quadrature conductivity measured at 1 Hz ( $\sigma''_{1Hz}$ ), the SIP normalized chargeability ( $m_n$ ), the NMR-estimated porosity ( $\phi_{NMR}$ ), the NMR mean-log transverse relaxation time ( $T_{2ml}$ ) and the NMR transverse relaxation time at the peak of the distribution ( $T_{2p}$ ).

16

	Clay %	Sample Name					SIP parameters			NMR parameters		
			$K$ (m/s)	$\phi$ (-)	$S_{por}$ ( $1/\mu\text{m}$ )	$F$ (-)	$\sigma'_{1Hz}$ (mS/m)	$\sigma''_{1Hz}$ (mS/m)	$m_n$ (mS/m)	$\phi_{NMR}$ (-)	$T_{2ml}$ (s)	$T_{2p}$ (s)
Homogeneous	0	H00A	$2.74 \times 10^{-4}$	0.39	0.16		28.2	--(b)	0.028	0.37	0.584	0.604
	0	H00B	$2.60 \times 10^{-4}$	0.40	0.14	5.92 <sub>(a)</sub>	29.8	0.017	0.118	0.37	0.606	0.649
	0	H00C	$2.11 \times 10^{-4}$	0.37	0.18		29.3	0.004	0.058	0.38	0.498	0.562
	1	H01A	$1.74 \times 10^{-4}$	0.37	0.70		28.2	0.042	0.421	0.37	0.356	0.487
	1	H01B	$1.41 \times 10^{-4}$	0.39	0.61	5.84 <sub>(a)</sub>	28.7	0.027	0.343	0.38	0.322	0.422
	1	H01C	$1.83 \times 10^{-4}$	0.39	0.57		28.9	0.021	0.259	0.38	0.384	0.476
	5	H05A	$4.95 \times 10^{-5}$	0.36	3.03		26.5	0.074	0.947	0.39	0.191	0.316
	5	H05B	$3.68 \times 10^{-5}$	0.37	2.69	4.24 <sub>(a)</sub>	28.6	0.062	0.901	0.41	0.179	0.274
	5	H05C	$4.63 \times 10^{-5}$	0.37	3.03		25.5	0.079	1.139	0.40	0.199	0.340
	10	H10A	$7.71 \times 10^{-6}$	0.36	5.27		26.4	0.107	1.782	0.40	0.103	0.073
	10	H10B	$6.12 \times 10^{-6}$	0.38	5.39	5.10 <sub>(a)</sub>	24.8	0.124	2.293	0.41	0.102	0.062
	10	H10C	$4.98 \times 10^{-6}$	0.37	6.26		24.1	0.092	1.812	0.36	0.096	0.070

	1	C01A	$2.83 \times 10^{-4}$	0.38	0.63	4.62	28.3	0.009	0.056	0.37	0.566	0.649
	1	C01B	$2.56 \times 10^{-4}$	0.39	0.68	4.78	30.0	-- <sup>(b)</sup>	0.030	0.38	0.614	0.698
	1	C01C	$2.17 \times 10^{-4}$	0.39	0.68	4.59	29.9	-- <sup>(b)</sup>	0.059	0.39	0.592	0.649
Clustered	5	C05A	$2.06 \times 10^{-4}$	0.38	2.99	4.51	29.8	-- <sup>(b)</sup>	0.320	0.37	0.426	0.649
	5	C05B	$2.12 \times 10^{-4}$	0.38	2.96	4.76	37.4	0.037	0.596	0.36	0.448	0.649
	5	C05C	$2.41 \times 10^{-4}$	0.39	2.83	4.54	28.9	0.015	0.257	0.39	0.458	0.649
	10	C10A	$2.21 \times 10^{-4}$	0.39	5.68	4.61	30.9	0.012	0.364	0.37	0.361	0.698
	10	C10B	$1.52 \times 10^{-4}$	0.39	5.30	4.27	29.8	0.062	0.441	0.38	0.332	0.604
	10	C10C	$1.80 \times 10^{-4}$	0.39	4.79	4.37	31.6	0.039	0.669	0.37	0.362	0.698

<sup>a</sup> Approximated  $F$  values from identically prepared samples with similar physical and geophysical properties.

<sup>b</sup> Measured phase angle below instrument resolution limit ( $<0.1$  mrad)

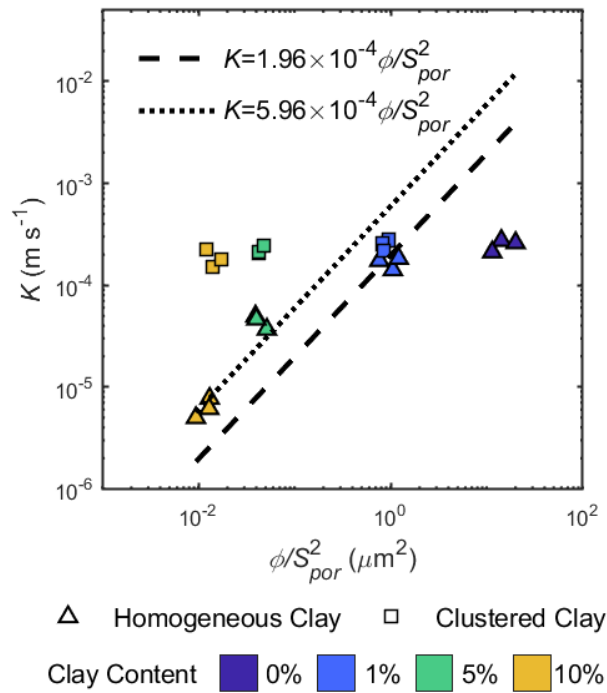
1

## 2 $K$ vs $S_{por}$

3 Figure 2 shows  $K$  plotted against  $\phi S_{por}^{-2}$  for all samples. For the data from the  
4 homogeneous samples, the fits are moderately good ( $A_{KC} = 1.96 \times 10^{-4}$  m/ $\mu\text{m}^2/\text{s}$  and  $NRMSE =$   
5  $0.393$ , see Table 2). The misfit largely results from the 0% clay samples; removing the 0% clay  
6 improves the fit ( $A_{KC} = 4.46 \times 10^{-4}$  m/ $\mu\text{m}^2/\text{s}$  and  $NRMSE = 0.22$ ). This shows that the Kozeny-  
7 Carman model (equation 2) effectively models the homogenous sample data for samples with  
8  $\geq 1\%$  clay by mass; however, at low clay contents ( $<1\%$  by mass), the clay may still have a large  
9 impact on the surface area but little to no impact on the hydraulic radius controlling  $K$ . When  
10 considering the data from both the homogeneous and clustered samples, we find that the model  
11 fits the data poorly ( $A_{KC} = 5.96 \times 10^{-4}$  m/ $\mu\text{m}^2/\text{s}$  and  $NRMSE = 0.507$ , see Table 2) as the model is  
12 not designed for highly heterogeneous samples. The values of  $A_{KC}$  calculated for the  
13 homogeneous samples and for all the samples are larger than the values given in Ozgumus et al.  
14 (2014) of  $4\text{--}14 \times 10^{-5}$  m/ $\mu\text{m}^2/\text{s}$ , which were compiled from a number of different studies. Thus, it  
15 appears that the samples from this study have lower tortuosity than the samples analyzed in the  
16 studies reported in Ozgumus et al. (2014).

1

2



3

4 Figure 2:  $K$  versus  $\phi/S_{por}^2$  for all samples. The dashed line and dotted lines show the fit of  
 5 Equation 2 to the homogeneous data and the entire dataset, respectively. The coefficients, ( $A_{KC}$ ),  
 6 and normalized root mean squared values are given in Table 2.

7

8 Table 2: Fitting coefficients and associated normalized root mean squared error ( $NRMSE$ ) values  
 9 from for the Kozeny-Carman  $K$  model (equation 2) shown in Figure 2. The coefficients for the  
 10 models are given for fits to the data from the homogeneous samples and for the fits to the data  
 11 from all samples. Units for the literature values were converted to the units of the fitting  
 12 coefficients.

Coefficients	Homogeneous Clay Samples	All Samples	Literature Values	Units	Equation	Figure
--------------	--------------------------	-------------	-------------------	-------	----------	--------

	Value	<i>NRMSE</i>	Value	<i>NRMSE</i>				
$A_{KC}$	$1.96 \times 10^{-4}$	0.393	$5.96 \times 10^{-4}$	0.507	$4-14 \times 10^{-5}^{(a)}$	m/ $\mu\text{m}^2/\text{s}$	2	1

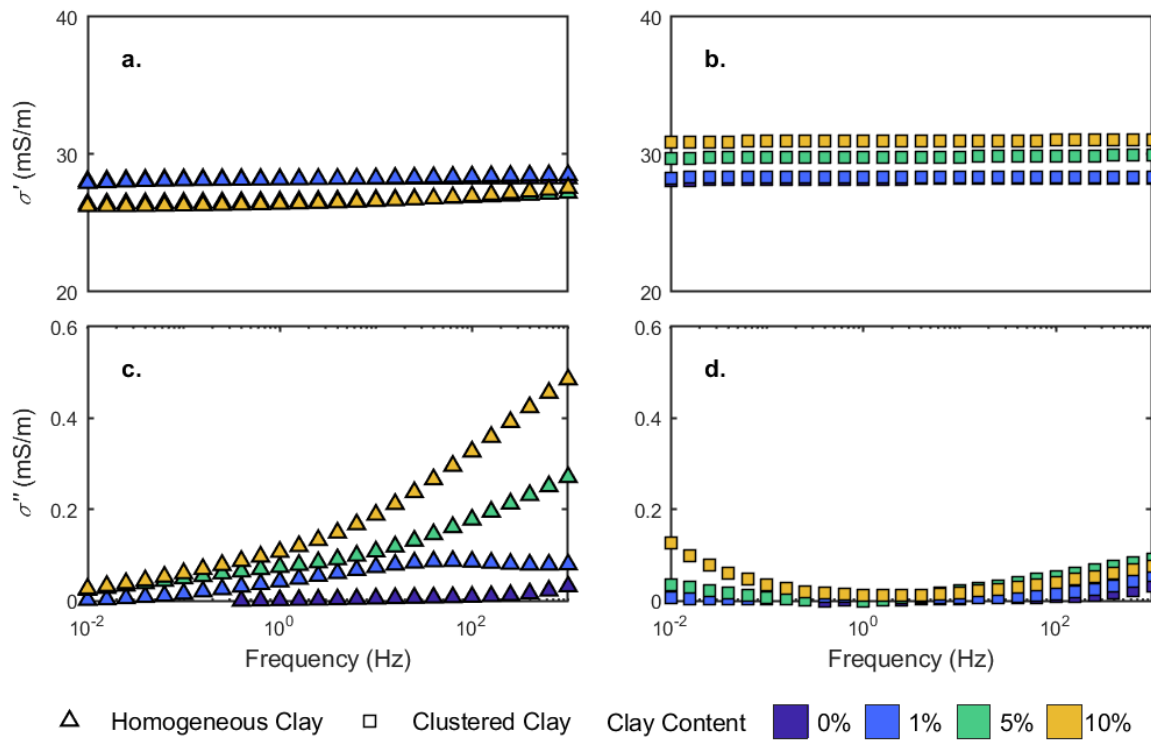
<sup>a</sup>Ozgumus et al. (2014); range of coefficients were compiled from sources cited within.

1

## 2 **Geophysical Results**

3 Figure 3 shows SIP spectra for representative homogeneous and clustered samples over  
4 the full range of clay content. Figures 3a and 3c shows  $\sigma'$  and  $\sigma''$  spectra, respectively, for H00A,  
5 H01A, H05A, and H10A, and Figures 3b and 3d shows  $\sigma'$  and  $\sigma''$  spectra, respectively, for  
6 H00A, C01A, C05A, and C10A. Overall, we do not observe any strong or consistent trends with  
7 increasing clay content on  $\sigma'$  for homogeneous or clustered clay samples and clay distribution  
8 does not appear to have a strong impact on  $\sigma'$  in the range of clay content tested. Increasing the  
9 homogeneous clay content causes an increase in  $\sigma''$  over the entire frequency spectrum,  
10 especially at frequencies above 100 Hz (Figure 3c), as expected from the literature (Okay et al.,  
11 2014). There is little increase in  $\sigma''$  with increasing clustered clay content (Figure 3d) in the  
12 intermediate frequency range (0.1 to 10 Hz), contrasting with the behavior seen for the  
13 homogeneous samples and suggesting that  $\sigma''$  is sensitive to clay distribution. At the low  
14 frequency range, we observe an increase in  $\sigma''$  with increasing clay content that is robust across  
15 replicate samples.





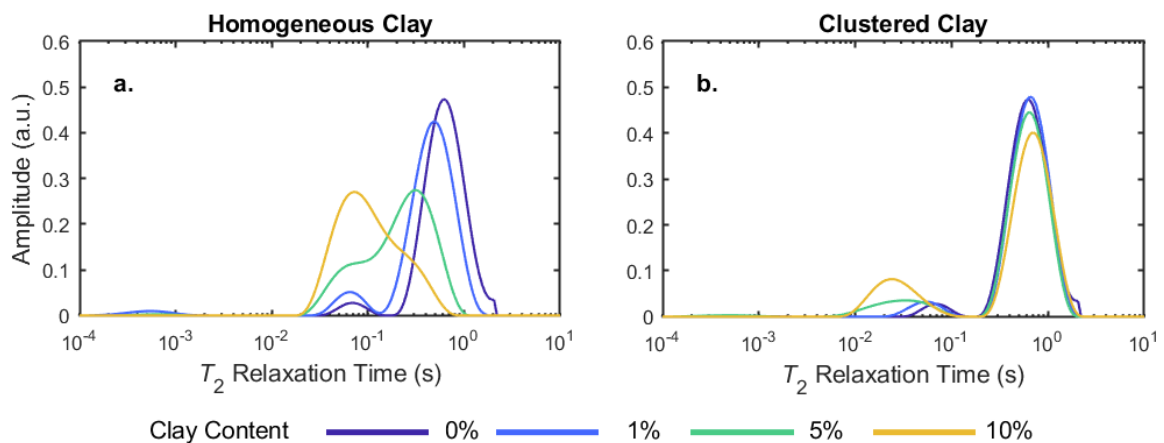
1

2 Figure 3: SIP data collected for representative homogeneous and clustered samples for each clay  
 3 content (samples H00A, H01A, H05A, and H10A shown in (a) and (c); samples H00A C01A,  
 4 C05A, and C10A shown in (b) and (d)). SIP  $\sigma'$  spectra for (a) homogeneous samples and (b)  
 5 clustered samples and SIP  $\sigma''$  spectra for (c) homogeneous samples and (d) clustered samples.

6 Figure 4 shows representative NMR  $T_2$  distributions for the homogeneous and clustered  
 7 samples over the entire range of clay content. Figure 4a shows  $T_2$  distributions for samples  
 8 H00A, H01A, H05A, and H10A, and Figure 4b shows  $T_2$  distributions for samples H00A, C01A,  
 9 C05A, and C10A. Increasing homogeneous clay content decreases the average pore size which  
 10 results in a shift in the dominantly mono-modal  $T_2$  distribution from long to shorter relaxation  
 11 times (Figure 4a). Similar results were shown by Anand et al. (2006) for homogeneous sand-  
 12 kaolinite mixtures and by Moss and Jing (2001) for homogeneous sand-montmorillonite and

1 sand-illite. In the clustered samples, increasing clay content results in the growth of a second,  
 2 short-relaxation time peak and a small decrease in the amplitude of the original peak (Figure 4b).  
 3 In the bimodal distribution, the long  $T_2$  peaks correspond to the large, sand-bound pores, and the  
 4 short  $T_2$  peaks correspond to the small, clay-bound pores. These results match well with the  $T_2$   
 5 distributions from the bimodal sediments studied in Anand et al. (2006) and the natural soils  
 6 studied by Stingaciu et al. (2009).

7 We note that, for the pure sand samples, relaxation was not entirely in the fast diffusion  
 8 regime ( $0.09 \leq \kappa \leq 1.25$ ) and so the second, short-relaxation time peak observed may represent a  
 9 second relaxation mode. This raises the possibility that some the signal in the shorter relaxation  
 10 times for the clustered samples may also represent faster relaxation modes in the pure-sand  
 11 portions of the sample in addition to the clay-bound water. For all other homogeneous samples,  $\kappa$   
 12  $< 0.1$ .



13  
 14 Figure 4: NMR  $T_2$  distributions for representative (a) homogenous samples and (b) clustered  
 15 samples from each clay content (samples H00A, H01A, H05A, and H10A shown in (a); samples  
 16 H00A C01A, C05A, and C10A shown in (b)).

1

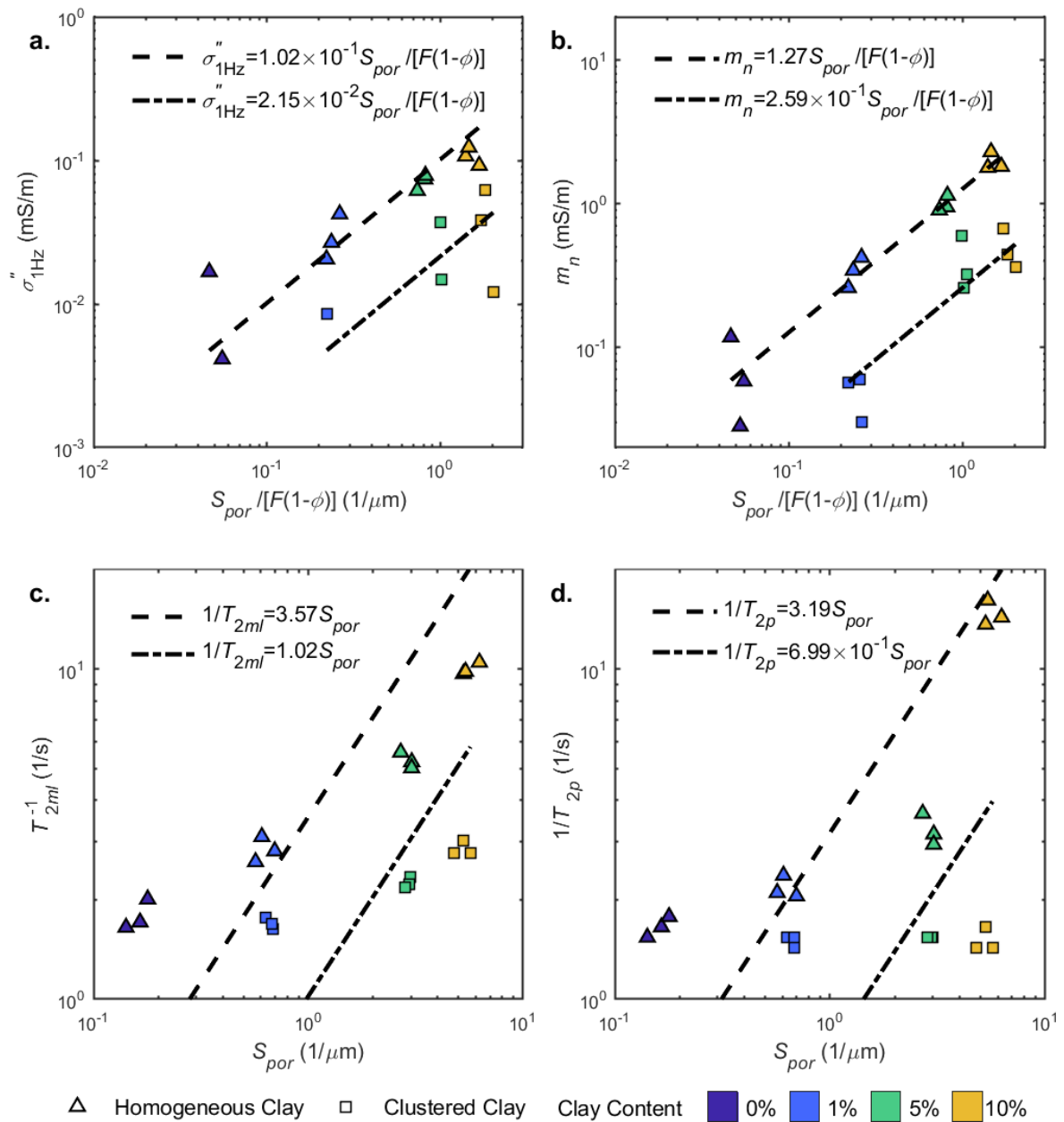
2 **Geophysical Parameters vs  $S_{por}$** 

3 Figure 5 shows characteristic geophysical parameters plotted versus pore geometric  
 4 parameters ( $S_{por}/[F(1-\phi)]$  in 5a and b,  $S_{por}$  in 5c and d). Here we compare the impact of clay  
 5 distribution on the relationship between the geophysical parameters and pore geometry by  
 6 calculating fitting coefficients for the homogeneous and clustered sample data separately. All  
 7 coefficients and *NRMSE* values for each fit are given in Table 3.

8 For the relationship between  $S_{por}/[F(1-\phi)]$  and  $\sigma''_{1\text{Hz}}$  (Figure 5a), we find a good fit for the  
 9 data from the homogeneous samples ( $C_s = 1.02 \times 10^{-1}$  mS um/m and *NRMSE*=0.139) and a  
 10 moderate fit for the data from the clustered samples ( $C_s = 2.15 \times 10^{-2}$  mS um/m and  
 11 *NRMSE*=0.336). When we examine the relationship between  $S_{por}/[F(1-\phi)]$  and  $m_n$  (Figure 5b),  
 12 we find there is an excellent fit for the data from the homogeneous samples ( $C_m = 1.27$  mS um/m  
 13 and *NRMSE*=0.0783) and a good fit for the data from the clustered samples ( $C_m = 0.259$  mS  
 14 um/m and *NRMSE*=0.140). The fitting coefficients,  $C_s$  and  $C_m$ , for the data from the  
 15 homogeneous samples are up to two times higher than values calculated from the literature; in  
 16 contrast, the fitted coefficients for the clustered data are slightly lower than values given in the  
 17 literature ( $C_s = 7.36 \times 10^{-2}$  and  $C_m = 5.96 \times 10^{-1}$  mS um/m from Revil et al., 2013; and Revil et al.,  
 18 2017). This indicates that the values of the  $C_s$  and  $C_m$  presented here represent endmember  
 19 values, where the high values correspond to homogeneous sand-clay media while the low values  
 20 correspond to heterogeneous media.

1           Considering the relationship between  $S_{por}$  and  $1/T_{2ml}$  (Figure 5c), we find that there is a  
2 moderately good fit for the data from the homogeneous samples ( $\rho_{2ml}=3.57$  m/s and  
3  $NRMSE=0.412$ ) and a poor fit for the data from the clustered sample ( $\rho_{2ml}=1.02$  m/s and  
4  $NRMSE=1.08$ ). Next when we consider the relationship between  $S_{por}$  and  $1/T_{2p}$  (Figure 5d), we  
5 find there is a moderately good fit for the data from the homogeneous ( $\rho_{2p}=3.20$  m/s and  
6  $NRMSE=0.341$ ), and a very poor fit for the data from the clustered samples ( $\rho_{2p}=6.99\times 10^{-1}$  m/s  
7 and  $NRMSE=6.04$ ). The values of  $\rho_{2ml}$  and  $\rho_{2p}$  for the data from the homogeneous samples are  
8 within the range reported in the literature for clean quartz samples and clean silicon carbide  
9 samples ( $\rho_2=3-5$   $\mu\text{m/s}$ , Kleinberg, 1996; Godefroy et al. 2001). Although the literature values of  
10  $\rho_2$  were calculated using  $T_{2ml}$ , we use them as an approximation of  $\rho_{2p}$ .

11



1

2 Figure 5: Characteristic geophysical parameters plotted versus pore geometric parameters: SIP  
 3 parameters  $\sigma''_{1\text{Hz}}$  (a) and  $m_n$  (b) versus  $S_{por}/[F(1-\phi)]$ ; NMR parameters  $1/T_{2ml}$  (c) and  $1/T_{2p}$  (d)  
 4 versus  $S_{por}$ . The dashed line shows the line of best fit for the data from the homogeneous  
 5 samples; the dot-dashed lines shows the line of best fit for the clustered samples, given by (a)

1 equation 6, (b) equation 10, and (c-d) equation 15. The coefficients  $C_s$  (a),  $C_m$  (b),  $\rho_{2ml}$  (c), and  
 2  $\rho_{2p}$  (d) were determined from fitting the  $\log_{10}$  parameters in a least-squared sense and are given  
 3 along with the corresponding normalized root mean squared values in Table 3.

4

5 Table 3: Fitting coefficients and associated normalized root mean squared error (*NRMSE*) values  
 6 for the petrophysical models given in Figure 5. Coefficients from the data from the homogeneous  
 7 samples are given separately from the coefficients determined from the data from the clustered  
 8 samples; the fits are shown as dashed lines and dot-dashed lines in Figure 5, respectively. Note  
 9 that the units listed are taken directly from the fits, and that the literature values have all been  
 10 converted to these units where necessary.

Coefficient	Homogeneous Clay Samples		Clustered Clay Samples		Literature Values	Units	Equation	Figure
	Value	<i>NRMSE</i>	Value	<i>NRMSE</i>				
$C_s$	$1.02 \times 10^{-1}$	0.139	$2.15 \times 10^{-2}$	0.336	$7.36 \times 10^{-2}$ <sup>(a)</sup>	mS um/m	6	5a
$C_m$	1.27	0.0783	$2.59 \times 10^{-1}$	0.140	$5.96 \times 10^{-1}$ <sup>(a)</sup>	mS um/m	10	5b
$\rho_{2ml}$	3.57	0.412	1.02	1.08	3–5 <sup>(b)</sup>	$\mu\text{m/s}$	15	5c
$\rho_{2p}$	3.20	0.341	$6.99 \times 10^{-1}$	6.04	3–5 <sup>(b)</sup>	$\mu\text{m/s}$	15	5d

<sup>a</sup> Values derived from coefficients given in Revil et al. (2013) and Revil et al., (2017).

<sup>b</sup> Godefroy et al. (2001); Kleinberg (1996); values given for silicon carbide and, at the low end, quartz sand.

11

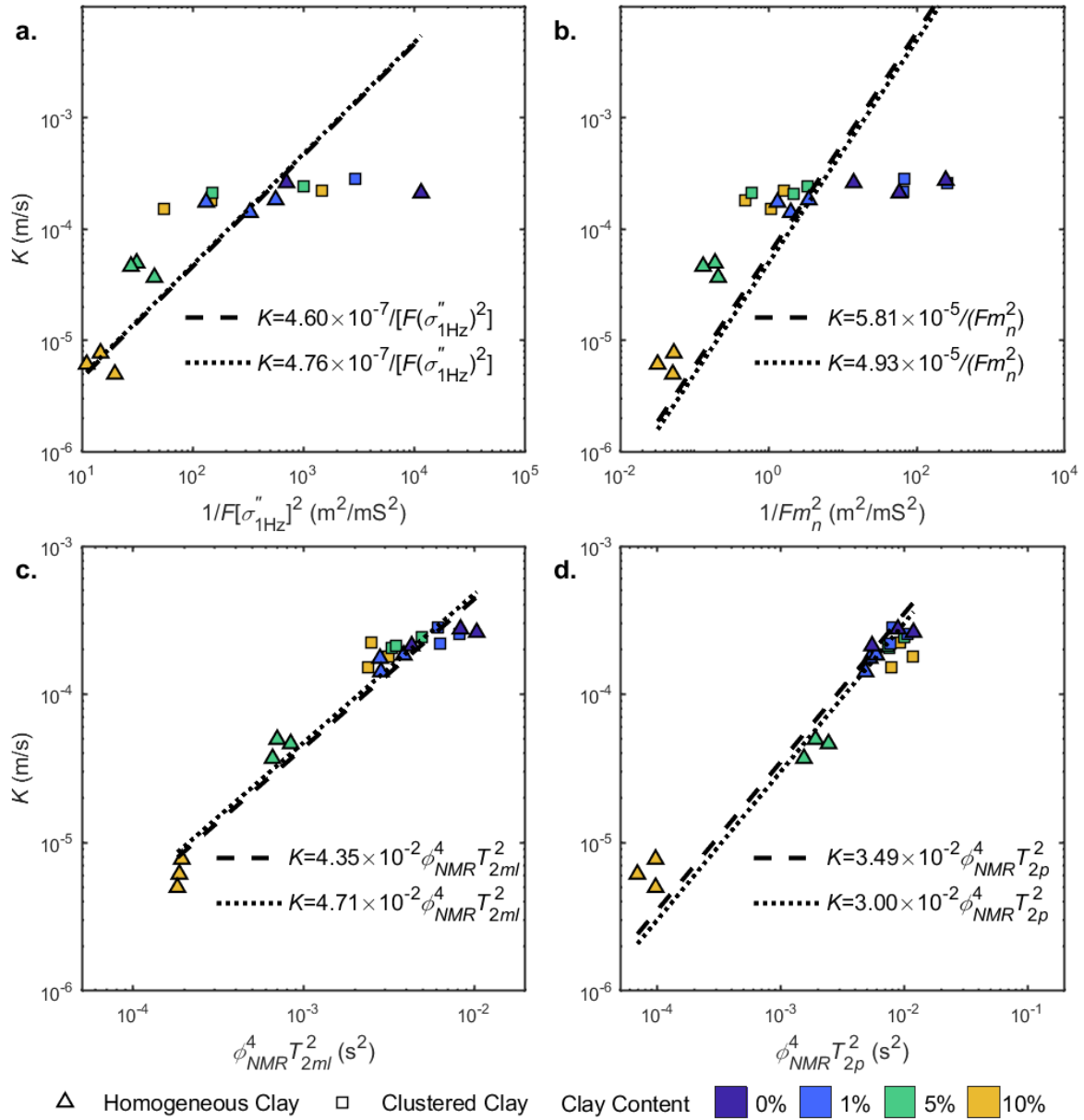
## 12 Geophysical Parameters vs $K$

13 Figure 6 shows  $K$  plotted versus characteristic geophysical parameters. The plot of  $K$   
 14 versus  $1/[F(\sigma''_{1\text{Hz}})^2]$  (Figure 6a) yields a moderately good fit for the data from the  
 15 homogeneous samples ( $A_s = 4.60 \times 10^{-7}$  mS<sup>2</sup>/m/s with *NRMSE*=0.301) as well as for the entire data  
 16 set ( $A_s = 4.76 \times 10^{-7}$  mS<sup>2</sup>/m/s with *NRMSE*=0.301). We do not fit the clustered samples alone in  
 17 Figure 6 alone as they do not demonstrate enough variation in  $K$  to extract meaningful statistics.  
 18 When we consider the relationship between  $K$  and  $1/[Fm_n^2]$  (Figure 6b) we observe moderately  
 19 good fits for the homogeneous sample data ( $A_m = 5.81 \times 10^{-5}$  mS<sup>2</sup>/m/s with *NRMSE*=0.424) and for

1 the entire dataset ( $A_m = 4.93 \times 10^{-5} \text{ mS}^2/\text{m/s}$  with  $NRMSE=0.466$ ). We observe that both fitting  
 2 coefficients  $A_s$  and  $A_m$  are remarkably consistent when fit to either the data from the  
 3 homogeneous samples or to data from both the homogeneous and clustered samples. All the  
 4 coefficients determined here are roughly half of the values from the literature ( $A_s = 1.19 \times 10^{-6}$   
 5  $\text{mS}^2/\text{m/s}$  and  $A_m = 9.55 \times 10^{-5} \text{ mS}^2/\text{m/s}$ , from Weller et al., 2010; Weller et al., 2015a). At high  $K$   
 6 ( $>10^{-4} \text{ m/s}$ ), we observe high variability in the SIP parameters but little variation in  $K$ ; these  
 7 values correspond to measurements collected on the pure sand and the clustered clay samples, so  
 8 this observation likely occurs because the SIP measurements on these samples are nearing the  
 9 instrument resolution. At lower  $K$  values, the SIP parameters vary more closely with  $K$ ;  
 10 recalculating fits for the homogeneous samples excluding the 0% clay samples yields good fits  
 11 ( $A_s = 6.74 \times 10^{-7} \text{ mS}^2/\text{m/s}$  with  $NRMSE=0.181$ , and  $A_m = 1.40 \times 10^{-4} \text{ mS}^2/\text{m/s}$  with  $NRMSE=0.159$ )  
 12 with fitted coefficients that are closer to the literature coefficients.

13 When plotting  $K$  versus  $\phi_{NMR}^4 T_{2ml}^2$  (Figure 6c), we find there are excellent fits for the data  
 14 from the homogeneous samples ( $B_{ml} = 4.35 \times 10^{-2} \text{ m/s}^3$  with  $NRMSE=0.0790$ ) and for the  
 15 combined dataset ( $B_{ml} = 4.71 \times 10^{-2} \text{ m/s}^3$  with  $NRMSE=0.0807$ ). When we plot  $K$  versus  $\phi_{NMR}^4 T_{2p}^2$   
 16 (Figure 6d), we observe good fits for both the data from the homogeneous samples ( $B_p = 3.49 \times 10^{-2}$   
 17  $\text{m/s}^3$  and  $NRMSE=0.116$ ) and for the combined dataset ( $B_p = 3.00 \times 10^{-2} \text{ m/s}^3$  with  
 18  $NRMSE=0.104$ ). The good-to-excellent fits derived for both the NMR parameters when using the  
 19 entire dataset result from the clustered clay samples all grouping near the high- $K$  limit of the  
 20 homogeneous samples. This grouping is expected from the  $T_2$ -distributions (Figure 4) where  
 21 there is little variation in dominant mode of the  $T_2$  distribution as clay content increases. The  
 22 values of  $B_{ml}$  and  $B_p$  determined here are substantially lower, by over an order of magnitude, than  
 23 the value found in the literature of  $B_{ml} = 0.8\text{--}4.70 \text{ m/s}^3$  (Maurer and Knight, 2016). This

- 1 difference likely arises due to mineralogical differences between the silica-kaolinite samples
- 2 studied here and the aquifer material studied in Maurer and Knight (2016).



3

4 Figure 6: Geophysical parameters plotted against  $K$ : SIP parameters  $1/F[\sigma''_{1\text{Hz}}]^2$  (a) and  $1/Fm_n^2$

5 (b); NMR parameters  $\phi_{NMR}^4 T_{2ml}^2$  (c) and  $\phi_{NMR}^4 T_{2p}^2$  (d). The dashed line and dotted lines show fitted



1  $K$ -models for the homogeneous data and the entire dataset, respectively, given by (a) equation  
 2 11, (b) equation 12, and (c-d) equation 16. The coefficients ((a)  $A_s$ , (b)  $A_m$ , (c)  $B_{ml}$  and (d)  $B_p$ ) and  
 3 normalized root mean squared values are given in Table 4.

4 Table 4: Fitting coefficients and associated normalized root mean squared error ( $NRMSE$ ) values  
 5 from for the  $K$  models shown in Figure 6. The coefficients for the models are given for fits to the  
 6 data just for the homogeneous samples and for the fits to the data from all samples. The units for  
 7 all values were converted to be consistent with the units used in this study.

Coefficients	Homogeneous Clay Samples		All Samples		Literature Values	Units	Equation	Figure
	Value	$NRMSE$	Value	$NRMSE$				
$A_s$	$4.60 \times 10^{-7}$	0.301	$4.76 \times 10^{-7}$	0.301	$1.19 \times 10^{-6}$ <sup>(a)</sup>	mS <sup>2</sup> /m/s	11	6a
$A_m$	$5.81 \times 10^{-5}$	0.424	$4.93 \times 10^{-5}$	0.466	$9.55 \times 10^{-5}$ <sup>(a)</sup>	mS <sup>2</sup> /m/s	12	6b
$B_{ml}$	$4.35 \times 10^{-2}$	0.0790	$4.71 \times 10^{-2}$	0.0807	0.80-4.70 <sup>(b)</sup>	m/s <sup>3</sup>	16	6c
$B_p$	$3.49 \times 10^{-2}$	0.116	$3.00 \times 10^{-2}$	0.104	0.80-4.70 <sup>(b)</sup>	m/s <sup>3</sup>	16	6d

<sup>a</sup>Weller et al. (2015a); approximate value from their equation 27 and Figure 5b.

<sup>b</sup>Maurer and Knight (2016); average value given for borehole measurements in aquifer.

8

9

## DISCUSSION

10 Our results demonstrate  $K$  is only well predicted from  $S_{por}$ , the proxy measure of clay  
 11 content, and  $\phi$  for the homogeneous samples. The clustered clay content had a minimal impact on  
 12  $K$  over the range of clay contents, which results in a poor fit when equation 2 is used to model to  
 13 the entire dataset. This result is expected as fluid should primarily flow through the hydraulically  
 14 interconnected sand matrix between the clay clusters and  $S_{por}$  is not a good proxy for the inverse  
 15 hydraulic radius in the clustered samples.

16 The SIP data are sensitive to changes in  $S_{por}$ , as both  $\sigma''_{1HZ}$  and  $m_n$  vary with  $S_{por}$  (Figures  
 17 5a and 5b) regardless of clay distribution. The linear correlation between the SIP parameters and  
 18  $S_{por}$  has been extensively documented in the literature in homogeneous samples (e.g. Revil and

1 Florsch, 2010; Weller et al., 2010, Revil et al., 2017), but not in heterogeneous material, such as  
2 the clustered samples reported here. The primary difference between the homogeneous and  
3 clustered samples is that the coefficients  $C_s$  and  $C_m$  are higher for the homogeneous samples than  
4 for the clustered samples, which supports the results of Wildenschild et al. (2000) who observed  
5 higher DC surface conduction in their homogeneous clay mixtures compared to their clustered  
6 clay samples. This makes sense as in-phase surface conductivity is known to be proportional to  
7 the quadrature conductivity (Börner et al., 1996; Weller et al. 2013). Sugand (2015) also  
8 observed higher quadrature conductivity in their homogeneous samples compared to their  
9 clustered samples. Based on equations 6 and 10, clustered samples and homogeneous samples  
10 with similar clay content, mineralogy, fluid chemistry, and saturation should theoretically  
11 produce similar  $\sigma''$  and  $m_n$  values. The decrease in these parameters for the clustered samples  
12 suggests there is a decrease in the electrical current density within the clay clusters. This  
13 indicates that the surface area available for polarization must be considered, where this “active  
14 surface area” is a function of the distribution of mineral grains in a porous medium.

15 In Figure 3d, we observe a clear and repeatable increase in signal amplitudes at  
16 frequencies lower than 1 Hz as a function of clay content. If the SIP measurement observes the  
17 clay clusters as very large, clay-coated grains experiencing EDL polarization, it is possible that a  
18 very low frequency (<0.01 Hz) peak would be associated with the clay clusters. Within the  
19 clusters, high clay content may lead to a reduction in the ionic mobility similar to what Weller et  
20 al. (2016) described for clay-bearing sandstones. These observations suggest that the active  
21 surfaces controlling the SIP spectra for the clustered clay samples may be isolated to the outer  
22 surfaces of the clusters. Tests at lower frequencies are necessary to confirm this hypothesis.

1           In the case of the homogeneous samples, the SIP data vary closely with  $K$ , especially  
2 when the 0% clay samples are removed. However, the SIP parameters for the clustered samples  
3 vary independently of  $K$  (Figures 6a and 6b). The non-negligible polarization of the clay clusters  
4 compromises the overall fit between the SIP parameters and  $K$  and suggests that the length scale  
5 controlling the SIP parameters may be more closely related to  $S_{por}$  than to the hydraulic radius in  
6 the sand-clay mixtures. Despite the polarization of the clay clusters, the SIP- $K$  models (Figures  
7 6a and 6b) still provide superior fits for both homogeneous and clustered clay sample data  
8 compared to the fits from the Kozeny-Carman equation (Figure 2). This suggests that the SIP  
9 active surface is a better proxy for the hydraulic radius than  $S_{por}$  in the tested samples.

10           Considering the NMR results, we find that the NMR relaxation times vary with  $S_{por}$   
11 (Figures 5c and 5d) for homogeneous samples but only give moderately good  $NRMSE$  values. At  
12 high clay content ( $\geq 5\%$ ) it appears that relationship between  $T_{2ml}$  and  $S_{por}$  for the homogeneous  
13 samples may become linear, suggesting that  $S_{por}$  may be a better proxy for inverse pore size at  
14 higher clay content. However, at low clay content ( $< 5\%$ ), the relationship appears nonlinear.  
15 This is likely because clay content variation at low clay contents ( $\leq 1\%$ ) will cause  
16 disproportionately large changes in surface area compared to pore size. These results  
17 demonstrate the potential pitfalls in applying  $T_{2ml}$  in equation 15 even in homogeneous sand-clay  
18 systems where  $S_{por}$  may not be an effective proxy for pore size. The relationship between  $T_{2p}$  and  
19  $S_{por}$  in Figure 5d is non-linear, indicating that  $T_{2p}$  is not an appropriate measure of  $S_{por}$  in the  
20 tested range.

21           For the clustered samples, there is no linear relationship between the NMR parameters  
22 and  $S_{por}$ . This follows from examining the bimodal  $T_2$  distributions in Figure 4b where the  $T_2$

1 peak, controlled by the sand-bound pores dominates the  $T_2$  distribution while  $S_{por}$  is primarily  
2 sensitive to the clay-bound surface area. This agrees with the results from Hinedi et al. (1997)  
3 who found that  $S_{por}$  in microporous silica beads was dominated by the microporosity that  
4 corresponded only to their fastest relaxation times. Further, our results support the findings of  
5 Stingaciu et al., (2009) who found that equation 15 could not be used to link the bimodal  $T_2$   
6 distributions to a bulk property like  $S_{por}$  in natural soils. It may instead be possible to represent  
7 the pore space more effectively using a weak-coupling relaxation model (Grunewald and Knight,  
8 2009; Keating and Knight, 2012) to distinguish between  $S_{por}$  in sand-bound and clay-bound pore  
9 space. Ultimately, the NMR results in Figures 5c and 5d highlight the disconnect between the  
10 NMR  $T_2$  distributions, which are sensitive to pore size distributions, and the bulk surface area  
11 measured by gas adsorption.

12         The distinct peaks in the clustered clay samples suggest there is little inter-pore coupling  
13 between the sand-bound water and the clay-bound water. We attribute this to the large size of the  
14 clay clusters, which reduce the probability that water molecules will diffuse through both clay-  
15 and sand-bound pores. This agrees with the findings of Grunewald and Knight (2009; 2011) who  
16 found that coarse heterogeneous sediments experienced less pore-coupling than fine-grained  
17 sediments. It is possible, however, that pore coupling would be observed in samples with smaller  
18 clay clusters or natural clay aggregates.

19         The fits between the NMR relaxation times and  $K$  (Figures 6c and 6d) are very good,  
20 consistently producing  $NRMSE$  values close to or less than 0.1 even when including the clustered  
21 sample data. The close fits show that the NMR parameters are better proxies of the hydraulic  
22 radius that controls  $K$  than that provided by  $S_{por}$  in the tested samples. However, care must be

1 taken when applying this result broadly, as NMR is a measure of bulk properties and is  
2 insensitive to anisotropy. Taking the laminated clay systems studied by Anand et al., (2006) as  
3 an example, if the laminations were oriented orthogonal to the hydraulic gradient, the hydraulic  
4 radius would be controlled by the clay-bound porosity rather than the sand-bound porosity. This  
5 means the shorter  $T_2$  peak would likely correspond to  $K$ . Since the  $T_2$  distribution contains no  
6 directional information, it is impossible to know which  $T_2$  peak contains the essential information  
7 about the hydraulic radius controlling  $K$  without additional information about pore connectivity.  
8 Thus, the non-uniqueness of the NMR response compromises its sensitivity to  $K$  in  
9 heterogeneous systems to a greater extent than our results indicate. Using pulsed-field gradient  
10 NMR methods to measure diffusional length scales (e.g. Latour et al., 1995) or combining the  
11 NMR measurements with additional measurements sensitive to anisotropy (e.g. SIP) may help to  
12 overcome this limitation.

13         The low variability in  $\phi$ ,  $\phi_{NMR}$ , and  $F$  indicate that these parameters do not have a strong  
14 impact on the  $K$  models. Excluding these parameters from the  $K$  models in equations 2, 11, 12,  
15 and 16 results in similar fitting coefficients and  $NRMSE$  values. These results support the  
16 findings of Weller et al. (2015a), who found that  $F$  could be excluded from SIP- $K$  models in  
17 unconsolidated materials, as well as the results of Maurer and Knight (2016), who showed that in  
18 unconsolidated aquifers that the  $n$  exponent in the SDR equation could be set to 0, negating the  
19 influence of  $\phi_{NMR}$ . In unconsolidated systems with little pore space tortuosity, there appears to be  
20 no need to include  $\phi$ ,  $\phi_{NMR}$ , or  $F$  in  $K$ -prediction models. A homogeneous, sandy system with low  
21 (<10%) clay content, such as the sand underlying the CFB Borden site in Canada (Sudicky and  
22 Illman, 2011), would likely satisfy these criteria.

1           We experimentally show that the sensitivity of SIP and NMR parameters to clay  
2 distribution in a sand matrix impacts the relationships between the physical and hydraulic  
3 parameters and the geophysical parameters. SIP parameters are linearly correlated to the clay  
4 content, with the correlation coefficient dependent on the clay distribution. The NMR relaxation  
5 time distributions are very sensitive to the distribution of pore sizes, resulting in very strong fits  
6 with  $K$ . As a result of their sensitivity to clay distribution, all geophysical parameters analyzed  
7 proved to be predictors of  $K$  rather than  $S_{por}$ , which is not sensitive to clay distribution. This  
8 suggests that geophysical methods may provide accurate field-scale estimates of  $K$  in  
9 heterogeneous geological environments where  $K$  models based on pore geometric parameters  
10 may be limited. Further study is necessary to understand the sensitivity of field SIP and NMR  
11 measurements to hydrogeological heterogeneity. This is particularly important for NMR  
12 measurements, which are only sensitive to bulk subsurface properties.

13           Future work should also focus on testing higher clay concentrations where the clusters  
14 may begin to impact  $K$ , different clay types expanding on the work of Anand et al. (2006) and  
15 Sugand (2015), and realistic geological analogs. The NMR results for the clustered samples in  
16 Figure 4b match closely with the laminated kaolinite samples from Anand et al. (2006),  
17 suggesting that they can be used to simulate systems where clay lenses are oriented parallel to  
18 the hydraulic gradient. However, further tests must be run to simulate a scenario where clay  
19 lenses are oriented orthogonally to the hydraulic gradient. Wildenschild et al. (2000) and Sugand  
20 (2015) have tested a small number of anisotropic sand-clay samples, observing that electrical  
21 measurements are sensitive to clay-lens orientation. Further tests on anisotropic clay distributions  
22 would provide an opportunity to better understand the sensitivity of SIP and NMR petrophysical

1 models to anisotropy. Such studies would help develop geophysical  $K$  models that are robust to  
2 varying clay distribution in addition to content and type.

3

4

## CONCLUSION

5 The quantity and distribution of kaolinite clay in synthetic sand-clay mixtures impacts the  
6 relationships between measured physical and hydraulic parameters and geophysical parameters.  
7 In homogeneous sand-clay samples, changes in clay content produce changes in hydraulic and  
8 geophysical parameters consistent with previous studies. When the clay is formed into large  
9 clusters, clay content no longer influences  $K$  and the geophysical responses become more  
10 complex. The SIP measurements are sensitive to increasing clay content as well as clay  
11 distribution and we find that the distribution of the clay controls the active surface area available  
12 for polarization. SIP estimates of  $K$  are overall superior to estimates from the Kozeny-Carman  
13 equation; however, variations in the SIP parameters in the clustered clay samples compromise  
14 the SIP- $K$  models. The NMR  $T_2$  distributions reflect the bimodal character of the pore space,  
15 with a second, short-time peak appearing with increasing clustered clay content. The  
16 characteristic NMR relaxation times do not closely track the increase in clay content but provide  
17 very accurate estimates of  $K$ , regardless of clay distribution. This suggests that the NMR  
18 parameters are more sensitive to the relevant hydraulic radius controlling  $K$  in these samples,  
19 compared to  $S_{por}$ , which is only sensitive for homogeneous samples. Further testing is required to  
20 understand how more geologically realistic clay distributions impact the relationships between  $K$   
21 and the measured geophysical parameters.





## 1 Glossary: Definitions and units of all symbols used.

Symbol	Definition	Units
$A$	NMR signal amplitude	arb
$A_0$	NMR initial signal amplitude	arb
CEC	Cation exchange capacity	C/kg
$f$	Stern layer partition coefficient	-
$F$	Archie's electrical formation factor	-
$f$	Frequency	Hz
$h$	NMR signal fraction	-
$k$	Permeability	m <sup>2</sup>
$K$	Hydraulic conductivity	m/s
$m$	Chargeability	-
$m_n$	Normalized chargeability	S/m
$m_t$	Total chargeability	-
<i>NRMSE</i>	Normalized root-mean square error	-
$n$	SDR porosity exponent	-
$Q_s$	Interfacial charge density at mineral surface	C/m <sup>2</sup>
$S_{por}$	Pore volume-normalized surface area	1/μm
$S_{SA}$	Specific surface area	m <sup>2</sup> /g
$T_2$	NMR transverse relaxation time	s
$T_{2B}$	NMR bulk water relaxation time	s
$T_{2S}$	NMR surface relaxation time	s
$T_{2D}$	NMR diffusion relaxation time	s
$T_{2ml}$	NMR mean-log relaxation time	s
$T_{2p}$	NMR relaxation time at $T_2$ distribution peak	s
$V$	Scaling factor between $K$ and $k$	m*s
$\alpha$	$\sigma''_{1Hz} \propto m_n$ proportionality constant	-
$\beta_{(+)}^S$	Ionic mobility in the Stern Layer	m <sup>2</sup> /s/V
$\phi$	Gravimetric porosity	(-)
$\phi_{NMR}$	NMR-estimated porosity	(-)
$\rho_g$	Matrix density	g/m <sup>3</sup>
$\sigma^*$	Complex electrical conductivity	S/m
$\sigma'$	Real electrical conductivity	S/m
$\sigma''$	Quadrature electrical conductivity	S/m
$ \sigma $	Complex electrical conductivity magnitude	S/m
$\sigma_0$	Conductivity at zero frequency	S/m
$\sigma_\infty$	Conductivity at high frequency asymptote	S/m
$\sigma''_{1Hz}$	Quadrature electrical conductivity at 1 Hz	S/m
$\sigma_f$	Conductivity of the saturating pore fluid	S/m
$\sigma_s'$	Real conductivity at the pore surface	S/m
$\theta$	Complex conductivity phase angle	rad
$\tau$	SIP relaxation time	s
Fitting Coefficients	Definition	Units
$A_{KC}$	Kozeny-Carman equation coefficient	m/μm <sup>2</sup> /s
$A_s/A_m$	SIP-hydraulic conductivity model coefficient	mS <sup>2</sup> /m/s
$B_m/B_p$	SDR equation coefficient	m/s <sup>3</sup>
$C_s / C_m$	SIP polarizability constant	mS um/m
$\rho_{2ml}/\rho_{2p}$	NMR surface relaxivity	m/s

## 1 APPENDIX A

2 Revil et al. (2017) define the following,

$$\sigma'' = \frac{1}{F\phi} \frac{\lambda}{\alpha} \rho_g \text{CEC}, \quad (\text{A1})$$

$$m_n = \frac{1}{F\phi} \lambda \rho_g \text{CEC}, \quad (\text{A2})$$

$$\lambda = \beta_{(+)}^S f, \quad (\text{A3})$$

3 Where  $\alpha$  is a unitless proportionality constant between  $\sigma''$  and  $m_n$ ,  $\rho_g$  is the grain density, the  
 4 CEC is the cation exchange capacity (C/kg),  $\beta_{(+)}^S$  is the ionic mobility of the counterions in the  
 5 Stern Layer ( $\text{m}^2/\text{s/V}$ ), and  $f$  is the partition coefficient describing the proportion of sorbed ions in  
 6 the Stern Layer. Revil et al. (2013) defines the cation exchange capacity as:

$$\text{CEC} = S_{sp} Q_s, \quad (\text{A4})$$

7 where  $Q_s$  is the charge density at the mineral surface ( $\text{C}/\text{m}^2$ ). Inserting A4 into equations A1 and  
 8 A2 and combining with equation 1 gives the following expressions,

$$\sigma'' = \frac{\beta_{(+)}^S f Q_s}{\alpha} \frac{S_{por}}{F(1-\phi)}, \quad (\text{A5})$$

$$m_n = \beta_{(+)}^S f Q_s \frac{S_{por}}{F(1-\phi)}, \quad (\text{A6})$$

9 where we define,

$$C_s = \frac{\beta_{(+)}^S f Q_s}{\alpha}, \quad (\text{A7})$$

$$C_m = \beta_{(+)}^S f Q_s. \quad (\text{A8})$$

1 Using  $\beta_{(+)}^S = 1.9 \times 10^{-9} \text{ m}^2/\text{s/V}$ ,  $f = 0.98$ ,  $Q_s = 0.32 \text{ C/m}^2$ , and  $\alpha = 8.1$  (Revil et al., 2013; Revil et  
2 al., 2017), and converting to the appropriate units described in the Spectral Induced Polarization  
3 Theory subsection, we find that  $C_s = 7.35 \times 10^{-2} \text{ mS}/\mu\text{m/m}$  and  $C_m = 5.96 \times 10^{-1} \text{ mS}/\mu\text{m/m}$ .

4

5

## REFERENCES

- 1
- 2 Archie, G., 1942, The electrical resistivity log as an aid in determining some reservoir  
3 characteristics: Transactions of the American Institute of Mining, Metallurgical, and  
4 Petroleum Engineers, **146**, 54–62.
- 5 Anand, V., G. J. Hirasaki, and M. Fleury, 2006, NMR diffusional coupling: effects of  
6 temperature and clay distribution, International Symposium of the Society of Core Analysts,  
7 doi: 10.1007/s00300-014-1595-6.
- 8 Anand, V., and G. J. Hirasaki, 2008, Paramagnetic relaxation in sandstones: distinguishing T1  
9 and T2 dependence on surface relaxation, internal gradients and dependence on echo  
10 spacing: Journal of Magnetic Resonance, **190**, 68–85, doi:10.1016/j.jmr.2007.09.019.
- 11 Banavar, J. R., and L. M. Schwartz, 1987, Magnetic resonance as a probe of permeability in  
12 porous media: Physical Review Letters, **58**, 1411–1414,  
13 doi:10.1103/PhysRevLett.58.1411.
- 14 Bear, J., 1972, Dynamics of Fluids in Porous Media, Vol. 1: American Elsevier Publishing  
15 Company.
- 16 Behroozmand, A., K. Keating, and E. Auken, 2015, A review of the principles and applications  
17 of the NMR technique for near-surface characterization: Surveys in Geophysics, **36**, 27–  
18 85, doi:10.1007/s10712-014-9304-0.
- 19 Binley, A., S. S. Hubbard, J. A. Huisman, A. Revil, D. A. Robinson, K. Singha, and L. D. Slater,  
20 2015, The emergence of hydrogeophysics for improved understanding of subsurface

- 1 processes over multiple scales: *Water Resources Research*, **51**, 3837–3866, doi:10.1002/  
2 2015WR017016.
- 3 Börner, F. D. J. R. Schopper, and A. Weller, 1996, Evaluation of transport and storage properties  
4 in the soil and groundwater zone from induced polarization measurements: *Geophysical*  
5 *Prospecting*, **44**, 583–601. <https://doi.org/10.1111/j.1365-2478.1996.tb00167.x>
- 6 Brownstein, K. R., and C. E. Tarr, 1979, Importance of classical diffusion in NMR studies of  
7 water in biological cells: *Physical Review A*, **19**, 2446– 2453, doi:  
8 10.1103/PhysRevA.19.2446.
- 9 Brunauer, S., P. H. Emmett, and E. Teller, 1938, Adsorption of gases in multimolecular layer:  
10 *Journal of the American Chemical Society*, **60**, 309–319, doi:10.1021/ja01269a023.
- 11 Bücker, M., and A. Hördt, 2013, Analytical modelling of membrane polarization with explicit  
12 parametrization of pore radii and the electrical double layer: *Geophysical Journal*  
13 *International*, **194**, 804–813, doi:10.1093/gji/ggt136.
- 14 Carman, P.C., 1939, Permeability of saturated sands, soils and clays: *The Journal of Agricultural*  
15 *Science*, **29**, 262-273. doi:10.1017/S0021859600051789.
- 16 Carrier, W. D., 2003, Goodbye, Hazen; Hello, Kozeny-Carman: *Journal of Geotechnical and*  
17 *Geoenvironmental Engineering*, **129**, 1054–1056, doi:10.1061/(ASCE)1090-  
18 0241(2003)129:11(1054).

- 1 Chapuis, R. P., and M. Aubertin, 2003, On the use of the Kozeny–Carman equation to predict the  
2 hydraulic conductivity of soils: *Canadian Geotechnical Journal*, **40**, 616–628,  
3 doi:10.1139/T03-013.
- 4 Coates, G. R., T. C. A. Peveraro, A. Hardwick, and D. Roberts, 1991, The magnetic resonance  
5 imaging log characterized by comparison with petrophysical properties and laboratory core  
6 data, paper presented at Society of Petroleum Engineers Annual Technical Conference and  
7 Exhibition.
- 8 Costabel, S., and U. Yaramanci, 2013, Estimation of water retention parameters from nuclear  
9 magnetic resonance relaxation time distributions: *Water Resources Research*, **49**, 2068–  
10 2079, doi:10.1002/wrcr.20207.
- 11 Daigle, H. and Dugan, B., 2009, Extending NMR data for permeability estimation in fine-  
12 grained sediments, *Marine and Petroleum Geology*, **26**, 1419–1427. doi:  
13 10.1016/j.marpetgeo.2009.02.008.
- 14 Daigle, H. and Dugan, B., 2011, An improved technique for computing permeability from NMR  
15 measurements in mudstones, *Journal of Geophysical Research: Solid Earth*, **116**, 1–14,  
16 doi: 10.1029/2011JB008353.
- 17 Dlubac, K., R. Knight, Y. Q. Song, N. Bachman, B. Grau, J. Cannia, and J. Williams, 2013, Use  
18 of NMR logging to obtain estimates of hydraulic conductivity in the High Plains aquifer,  
19 Nebraska, USA: *Water Resources Research*, **49**, 1871–1886, doi:10.1002/wrcr.20151.

- 1 Dlugosch, R., T. Günther, M. Müller-Petke, and U. Yaramanci, 2013, Improved prediction of  
2 hydraulic conductivity for coarse-grained, unconsolidated material from nuclear magnetic  
3 resonance: *Geophysics*, **78**, EN55-EN64, doi:10.1190/geo2012-0187.1.
- 4 Domenico, P. A., and F. W. Schwartz, 1990, *Physical and Chemical Hydrogeology*: John Wiley.
- 5 Foley, I., S. Farooqui, and R. Kleinberg, 1996, Effect of Paramagnetic Ions on NMR Relaxation  
6 of Fluids at Solid Surfaces: *Journal of Magnetic Resonance A*, **123**, 95–104,  
7 doi:10.1006/jmra.1996.0218.
- 8 Grunewald, E., and R Knight, 2009, A Laboratory Study of NMR Relaxation Times and Pore  
9 Coupling in Heterogeneous Media: *Geophysics*, **74**, E215, doi: 10.1190/1.3223712.
- 10 Grunewald, E., and R. Knight, 2011, A laboratory study of NMR relaxation times in  
11 unconsolidated heterogeneous sediments. *Geophysics*, **76**, G73–G83, doi:  
12 10.1190/1.3581094.
- 13 Godefroy, S., J.-P. Korb, M. Fleury, and R. & Bryant, 2001, Surface nuclear magnetic relaxation  
14 and dynamics of water and oil in macroporous media: *Physical Review E*, **64**, 21605, doi:  
15 10.1103/PhysRevE.64.021605.
- 16 Hinedi, Z. R., A. C. Chang, M. A. Anderson, and D. B. Borchardt, 1997, Quantification of  
17 microporosity by nuclear magnetic resonance relaxation of water imbibed in porous media,  
18 *Water Resources Research*, **33**, 2697–2704, doi: 10.1029/97WR02408.

- 1 Howard J., and W. Kenyon, 1992, Determination of pore size distribution in sedimentary rocks  
2 by proton nuclear magnetic resonance. *Marine and Petroleum Geology*, **9**, 139-145, doi:  
3 10.1016/0264-8172(92)90086-T.
- 4 Johnson, D., J. Koplik, and L. Schwartz, 1986, New pore-size parameter characterizing transport  
5 in porous media: *Physical Review Letters*, **57**, 2564–2567, doi:  
6 10.1103/PhysRevLett.57.2564.
- 7 Keating, K., and R. Knight, 2007, A laboratory study to determine the effect of iron oxides on  
8 proton NMR measurements: *Geophysics*, **72**, E27–E32, doi:10.1190/1.2399445.
- 9 Keating, K., R. Knight, 2012, The effect of spatial variation in surface relaxivity on nuclear  
10 magnetic resonance relaxation rates: *Geophysics*, **77**, E365–E377,  
11 <https://doi.org/10.1190/geo2011-0462.1>.
- 12 Keating, K., 2014, A laboratory study to determine the effect of surface area and bead diameter  
13 on NMR relaxation rates of glass bead packs: *Near Surface Geophysics*, **12**, 243–254,  
14 doi:10.3997/1873-0604.2013064.
- 15 Keery, J., A. Binley, A. Elshenawy, and J. Clifford, 2012, Markov-chain Monte Carlo estimation  
16 of distributed Debye relaxations in spectral induced polarization: *Geophysics*, **77**, E159,  
17 doi:10.1190/geo2011-0244.1.
- 18 Keller, C. K., G. Van Der Kamp, and J. A. Cherry, 1989, A multiscale study of the permeability  
19 of a thick clayey till: *Water Resources*, **25**, 2299–2317, doi:10.1029/WR025i011p02299.



- 1 Kemna, A., A. Binley, C. Giorgio, E. Niederleithinger, A. Revil, L. Slater, K. H. Williams, A. F.  
2 Orozco, F. Haegel, A. Hördt, S. Kruschwitz, V. Leroux, K. Titov, E. Zimmermann.,  
3 2012, An overview of the spectral induced polarization method for near-surface  
4 applications: *Near Surface Geophysics*, **10**, 453–468, doi:10.3997/1873-0604.2012027.
- 5 Kenyon W., R. Kleinberg, C. Straley, 1995, Nuclear Magnetic Resonance Imaging: Technology  
6 for the 21st Century. *Oilfield Review*, **7**, 19-33.
- 7 Kleinberg, R. L., 1996, Utility of NMR  $T_2$  distributions, connection with capillary pressure, clay  
8 effect, and determination of the surface relaxivity parameter  $\rho_2$ : *Magnetic Resonance*  
9 *Imaging*, **14**, 761–767.
- 10 Kleinberg, R. L., and M. A. Horsfield, 1990, Transverse relaxation processes in porous  
11 sedimentary rock: *Journal of Magnetic Resonance*, **88**, 9–19, doi:10.1016/0022-  
12 2364(90)90104-H.
- 13 Latour, L. L., R. L. Kleinberg, P. P. Mitra, and C. H. Sotak, 1995, Pore-size distributions and  
14 tortuosity in heterogeneous porous media, *Journal of Magnetic Resonance, Series A*, **112**,  
15 83-91, doi: 10.1006/jmra.1995.1012.
- 16 Leroy, P., A. Revil, Kemna, P. Cosenza, and A. Ghorbani, 2008, Complex conductivity of water-  
17 saturated packs of glass beads: *Journal of Colloid Interface Science*, **321**, 103–17, doi:  
18 10.1016/j.jcis.2007.12.031.
- 19 Marshall, D. J., and T. R. Madden, 1959, Induced polarization, a study of its causes: *Geophysics*,  
20 **24**, 790–816, doi:10.1190/1.1438659.

- 1 Maurer, J., and R. Knight, 2016, Models and methods for predicting hydraulic conductivity in  
2 near-surface unconsolidated sediments using nuclear magnetic resonance: *Geophysics*, **81**,  
3 D503–D518, doi:10.1190/geo2015-0515.1.
- 4 Meiboom, S., and D. Gill, 1958, Modified spin-echo method for measuring nuclear relaxation  
5 times: *The Review of Scientific Instruments*, **29**, 688–691, doi:10.1063/1.1716296.
- 6 Minagawa, H., Y. Nishikawa, I. Ikeda, K. Miyazaki, N. Takahara, Y. Sakamoto, T. Komai, and  
7 H. Narita, 2008, Characterization of sand sediment by pore size distribution and  
8 permeability using proton nuclear magnetic resonance measurement: *Journal of*  
9 *Geophysical Research*, **113**, B07210, doi:10.1029/2007JB005403.
- 10 Moss, A., and X. Jing, 2001, An investigation into the effect of clay type, volume and  
11 distribution on NMR measurements in sandstones, Society of Core Analysts Symposium.
- 12 Morriss, C., D. Rossini, C. Straley, P. Tutunjian, and H. Vinegar, 1997, Core analysis by low-  
13 field NMR, *The Log Analyst*, **38**.
- 14 Neuzil, C. E., 1986, Groundwater Flow in Low-Permeability Environments: *Water Resources*  
15 *Research*, **22**, 1163–1195, doi:10.1029/WR022i008p01163.
- 16 Nordsiek, S., and A. Weller, 2008, A new approach to fitting induced-polarization spectra:  
17 *Geophysics*, **73**, F235–F245, doi:10.1190/1.2987412.
- 18 Nordsiek, S., E. Diamantopoulos, A. Hördt, and W. Durner, 2016, Relationships between soil  
19 hydraulic parameters and induced polarization spectra: *Near Surface Geophysics*, **14**, 23–  
20 37, doi:10.3997/1873-0604.2015050.

- 1 Ntarlagiannis, D. and L. Slater, 2014, Quantifying the Accuracy of Laboratory SIP Experimental  
2 Set Ups: Presented at the 2014 Fall Meeting, AGU.
- 3 Okay, G., P. Leroy, A. Ghorbani, P. Cosenza, C. Camerlynck, J. Cabrera, N. Florsch, and A.  
4 Revil, 2014, Spectral induced polarization of clay-sand mixtures: Experiments and  
5 modeling: *Geophysics*, **79**, E353–E375, doi:10.1190/geo2013-0347.1.
- 6 Osterman, G., K. Keating, A. Binley, and L. D. Slater, 2016, A laboratory study to estimate pore  
7 geometric parameters of sandstones using complex conductivity and nuclear magnetic  
8 resonance for permeability prediction: *Water Resources Research*, **52**, 4321–4337,  
9 doi:10.1002/2015WR018472.
- 10 Ozgumus, T., M. Mobedi, and U. Ozkol, 2014, Determination of Kozeny constant based on  
11 porosity and pore to throat size ratio in porous medium with rectangular rods:  
12 *Engineering Applications of Computational Fluid Mechanics*, **52**, 308-318,  
13 doi:10.1080/19942060.2014.11015516.
- 14 Palacky, G. J., 1987, Clay mapping using electromagnetic methods: *First Break*, **5**, 295-306, doi:  
15 10.3997/1365-2397.1987015.
- 16 Pape, H., L. Riepe, and J. R. Schopper, 1987, Interlayer conductivity of rocks - a fractal model of  
17 interface irregularities for calculating interlayer conductivity of natural porous mineral  
18 systems: *Colloids and Surfaces*, **27**, 97–122, doi:10.1016/0166-6622(87)80331-1.
- 19 Revil, A., and L. M. Cathles, 1999, Permeability of shaly sands: *Water Resources Research*, **35**,  
20 651–662, doi:10.1029/98WR02700.

- 1 Revil, A., and N. Florsch, 2010, Determination of permeability from spectral induced  
2 polarization in granular media: *Geophysical Journal International*, **181**, 1480–1498,  
3 doi:10.1111/j.1365-246X.2010.04573.x.
- 4 Revil, A., 2012, Spectral induced polarization of shaly sands: Influence of the electrical double  
5 layer: *Water Resources Research*, **48** W02517, doi: 10.1029/2011WR011260.
- 6 Revil, A., 2013, On charge accumulation in heterogeneous porous rocks under the influence of  
7 an external electric field: *Geophysics*, **78**, D271–D291, doi:10.1190/geo2012-0503.1.
- 8 Revil, A., J. D. Eppehimer, M. Skold, M. Karaoulis, L. Godinez, and M. Prasad, 2013, Low-  
9 frequency complex conductivity of sandy and clayey materials. *Journal of Colloid and*  
10 *Interface Science*, **398**, 193–209, doi:10.1016/j.jcis.2013.01.015.
- 11 Revil, A., A. Binley, L. Mejus, and P. Kessouri, 2015, Predicting permeability from the  
12 characteristic relaxation time and intrinsic formation factor of complex conductivity  
13 spectra, *Water Resources Research*, **51**, 6672–6700, doi:10.1002/2015WR017074.
- 14 Revil, A., A. Coperey, A. Shao, N. Florsch, I. L. Fabricius., Y. Deng, J. R. Delsman, P. S. Pauw,  
15 M. Karaoulis, P. G. B. de Louw, E.S. van Baaren, W. Dabekaussen, A. Menkovic, and J.  
16 L. Gunnink, 2017, Complex conductivity in soils: *Water Resources Research*, **53**, 5121-  
17 7147, doi: 10.1002/2017WR020655.
- 18 Ryu, S., 2009, Effect of inhomogeneous surface relaxivity, pore geometry and internal field  
19 gradients on NMR logging: Exact and perturbative theories and numerical investigations:  
20 presented at SPWLA 50th Annual Logging Symposium.

- 1 Seevers, D. O., 1966, A nuclear magnetic method for determining the permeability of  
2 sandstones, 7th Annual Logging Symposium: presented at Society of Petrophysical Well  
3 Log Analysts.
- 4 Sen, P. N., P. A. Goode, and A. Sibbit, 1988, Electrical conduction in clay bearing sandstones at  
5 low and high salinities: *Journal of Applied Physics*, **63**, pp.4832-4840, doi:  
6 10.1063/1.340476.
- 7 Slater, L. D., and D. R. Glaser, 2003, Controls on induced polarization in sandy unconsolidated  
8 sediments and application to aquifer characterization: *Geophysics*, **68**, 1547–1558,  
9 doi:10.1190/1.1620628.
- 10 Slater, L., D. Ntarlagiannis, and D. Wishart, 2006, On the relationship between induced  
11 polarization and surface area in metal-sand and clay-sand mixtures: *Geophysics*, **71**, A1–  
12 A5, doi:10.1190/1.2187707.
- 13 Slater, L., 2007, Near surface electrical characterization of hydraulic conductivity: from  
14 petrophysical properties to aquifer geometries—a review: *Surveys in Geophysics*, **28**,  
15 169–197, doi:10.1007/s10712-007-9022-y.
- 16 Stingaciu, L. R., A. Pohlmeier, P. Blümler, L. Weihermüller, D. van Dusschoten, S. Stapf, and  
17 H. Vereecken, 2009, Characterization of unsaturated porous media by high-field and low-  
18 field NMR relaxometry: *Water Resources Research*., **45**, W08412,  
19 doi:10.1029/2008WR007459.

- 1 Sudicky, E. A., and W. A. Illman, 2011, Lessons learned from a suite of CFB Borden  
2 experiments. *Groundwater*, **49**, 630–48, doi.org/10.1111/j.1745-6584.2011.00843.x.
- 3 Sugand M. G., 2015, Effect of microstructural variation on hydrogeophysical properties of  
4 unconsolidated sand – clay mixtures: M.S. thesis, Lancaster University.
- 5 Swanson, R. D., A. Binley, K. Keating, S. France, G. Osterman, F. D. Day-Lewis, and K.  
6 Singha, 2015, Anomalous solute transport in saturated porous media: relating transport  
7 model parameters to electrical and nuclear magnetic resonance properties, *Water Resources*  
8 *Research*, **51**, 1264–1283, doi: 10.1002/2014WR015284
- 9 Sumner, J. S., 1976, Principles of induced polarization for geophysical exploration: Elsevier,  
10 New York, NY.
- 11 Timur, A., 1969, Pulsed nuclear magnetic resonance studies of porosity, movable fluid, and  
12 permeability of sandstones: *Society of Petroleum Engineers*, 21, 775-786,  
13 doi:10.2118/2045-PA.
- 14 Titov, K., V. Komarov, V. Tarasov, and A. Levitski, 2002, Theoretical and experimental study of  
15 time domain-induced polarization in water-saturated sands: *Journal of Applied Geophysics*,  
16 **50**, 417–433, doi:10.1016/S0926-9851(02)00168-4.
- 17 Vinegar, H. J., and M. H. Waxman, 1984, Induced polarization of shaly sands: *Geophysics*, **49**,  
18 1267–1287, doi:10.1190/1.1441755.

- 1 Wallace, D. W., 2015, A laboratory study to develop a permeability model for unconsolidated  
2 glass bead packs by combining NMR and SIP measured parameters: M.S. thesis, Rutgers  
3 University-Newark.
- 4 Weller, A., L. Slater, S. Nordsiek, and D. Ntarlagiannis, 2010, On the estimation of specific  
5 surface per unit pore volume from induced polarization: a robust empirical relation fits  
6 multiple data sets: *Geophysics*, **75**, WA105–WA112. doi:10.1190/1.3471577.
- 7 Weller, A.; Breede, K.; Slater, L.; Nordsiek, S. 2011, Effect of changing water salinity on  
8 complex conductivity spectra: *Geophysics* **76**, No. 6, F315-F327, doi:  
9 10.1190/GEO2011-0072.1
- 10 Weller, A., L. Slater, and S. Nordsiek, 2013, On the relationship between induced polarization  
11 and surface conductivity: implications for petrophysical interpretation of electrical  
12 measurements: *Geophysics*, **78**, D315–325, doi:10.1190/geo2013-0076.
- 13 Weller and Slater, 2015, Induced polarization dependence on pore space geometry: Empirical  
14 observations and mechanistic predictions: *Journal of Applied Geophysics*, **123**, 310-315,  
15 doi: 10.1016/j.jappgeo.2015.09.002.
- 16 Weller, A., L. Slater, A. Binley, S. Nordsiek, and S. Xu, 2015a, Permeability prediction based on  
17 induced polarization: Insights from measurements on sandstone and unconsolidated  
18 samples spanning a wide permeability range: *Geophysics*, **80**, D161–D173,  
19 doi:10.1190/GEO2014-0368.1.

- 1 Weller, A.; L. Slater, J. A. Huisman, O. Esser, F.-H. Haegel, 2015b, On the specific  
2 polarizability of sands and sand-clay mixtures. *Geophysics* **80**, A57-A61, doi:  
3 10.1190/geo2014-0509.1.
- 4 Whittall, K. P., M. J. Bronskill, and R. M. Henkelman, 1991, Investigation of analysis techniques  
5 for complicated NMR relaxation data: *Journal of Magnetic Resonance*, **95**, 221–234,  
6 doi:10.1016/0022-2364(91)90213-D.
- 7 Wildenschild, D., J. J. Roberts, and E. D. Carlberg, 2000, On the relationship between  
8 microstructure and electrical and hydraulic properties of sand-clay mixtures: *Geophysical*  
9 *Research Letters*, **27**, 3085–3088, doi:10.1029/2000GL011553.
- 10 Zisser, N., A. Kemna, and G. Nover, 2010, Relationship between low-frequency electrical  
11 properties and hydraulic permeability of low-permeability sandstones: *Geophysics*, **75**,  
12 E131–E141, doi:10.1190/1.3413260.

13

14



## LIST OF FIGURES

1

2

3 Figure 1: Examples of dry samples prior to packing, (a) 90% sand mixed homogeneously with  
 4 10% clay; (b) 90% sand mixed with 10% clay clustered in ~5 mm balls; (c) clay clusters shown  
 5 with a US quarter for scale.

6

7 Figure 2:  $K$  versus  $\phi/S_{por}^2$  for all samples. The dashed line and dotted lines show the fit of  
 8 Equation 2 to the homogeneous data and the entire dataset, respectively. The coefficients,  $(A_{KC})$ ,  
 9 and normalized root mean squared values are given in Table 2.

10

11 Figure 3: SIP data collected for representative homogeneous and clustered samples for each clay  
 12 content (samples H00A, H01A, H05A, and H10A shown in (a) and (c); samples H00A C01A,  
 13 C05A, and C10A shown in (b) and (d)). SIP  $\sigma'$  spectra for (a) homogeneous samples and (b)  
 14 clustered samples and SIP  $\sigma''$  spectra for (c) homogeneous samples and (d) clustered samples.

15

16 Figure 4: NMR  $T_2$  distributions for representative (a) homogenous samples and (b) clustered  
 17 samples from each clay content (samples H00A, H01A, H05A, and H10A shown in (a); samples  
 18 H00A C01A, C05A, and C10A shown in (b)).

19

20 Figure 5: Characteristic geophysical parameters plotted versus pore geometric parameters: SIP  
 21 parameters  $\sigma''_{1Hz}$  (a) and  $m_n$  (b) versus  $S_{por}/[F(1-\phi)]$ ; NMR parameters  $1/T_{2ml}$  (c) and  $1/T_{2p}$  (d)

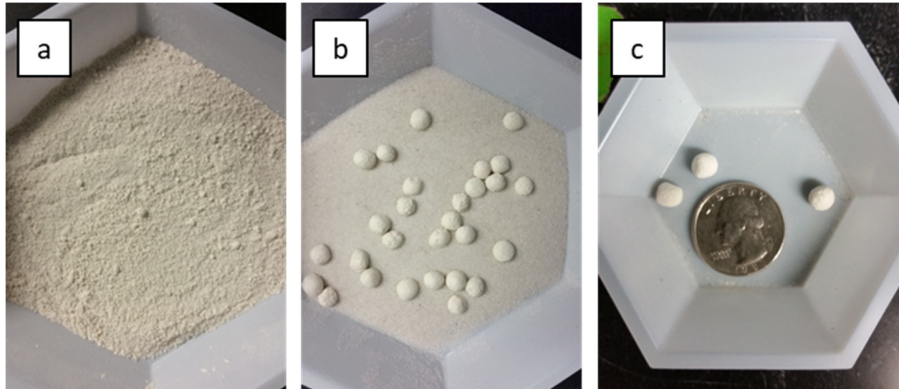
1 versus  $S_{por}$ . The dashed line shows the line of best fit for the data from the homogeneous  
 2 samples; the dot-dashed lines shows the line of best fit for the clustered samples, given by (a)  
 3 equation 6, (b) equation 10, and (c-d) equation 15. The coefficients  $C_s$  (a),  $C_m$  (b),  $\rho_{2ml}$  (c), and  
 4  $\rho_{2p}$  (d) were determined from fitting the  $\log_{10}$  parameters in a least-squared sense and are given  
 5 along with the corresponding normalized root mean squared values in Table 3.

6

7 Figure 6: Geophysical parameters plotted against  $K$ : SIP parameters  $1/F[\sigma''_{1Hz}]^2$  (a) and  $1/F m_n^2$   
 8 (b); NMR parameters  $\phi_{NMR}^4 T_{2ml}^2$  (c) and  $\phi_{NMR}^4 T_{2p}^2$  (d). The dashed line and dotted lines show fitted  
 9  $K$ -models for the homogeneous data and the entire dataset, respectively, given by (a) equation  
 10 11, (b) equation 12, and (c-d) equation 16. The coefficients ((a)  $A_s$ , (b)  $A_m$ , (c)  $B_{ml}$  and (d)  $B_p$ ) and  
 11 normalized root mean squared values are given in Table 4.

12

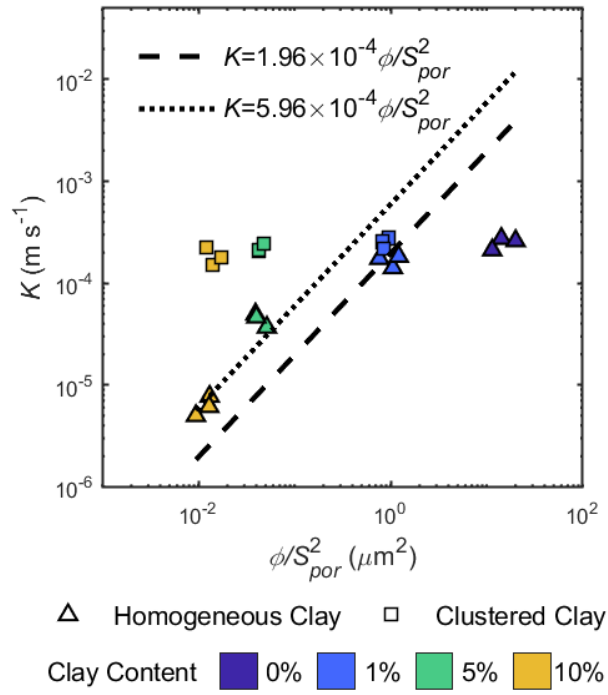
13



1

2 Figure 1

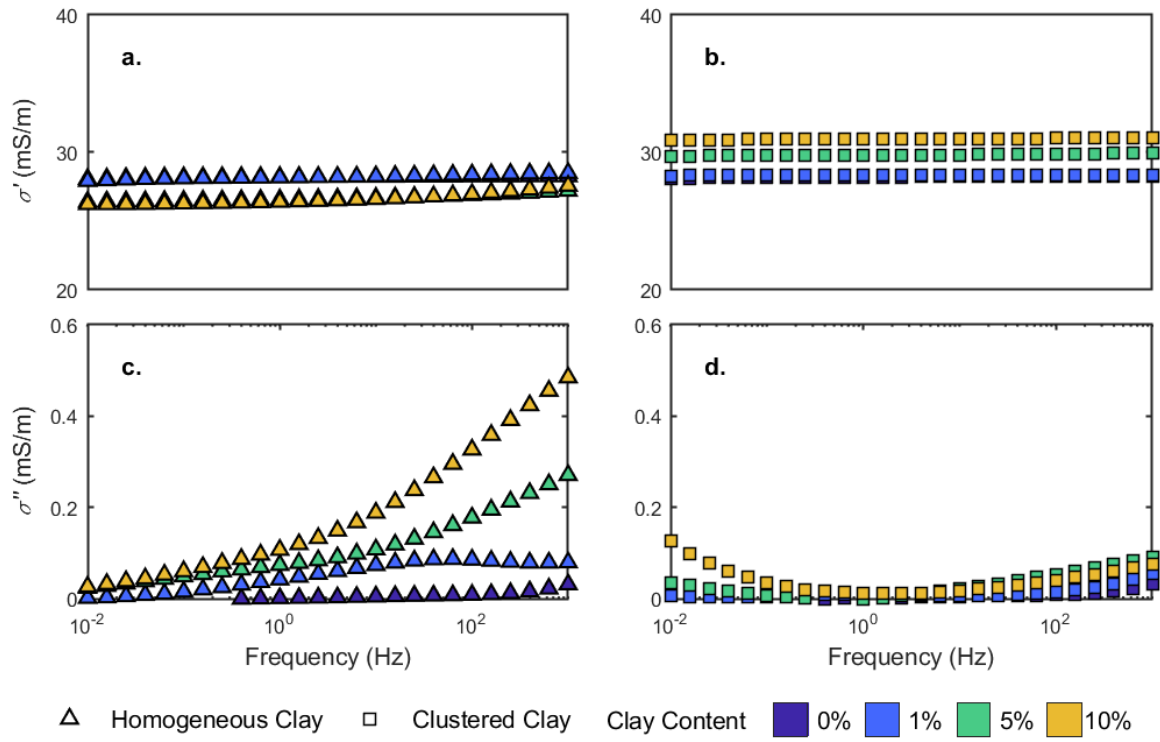
3



1

2 Figure 2

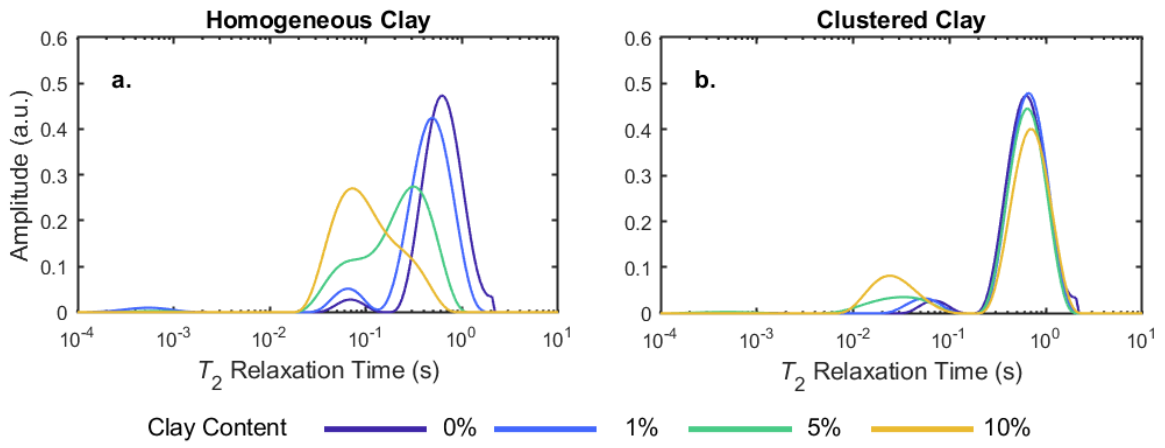
3



1

2 Figure 3

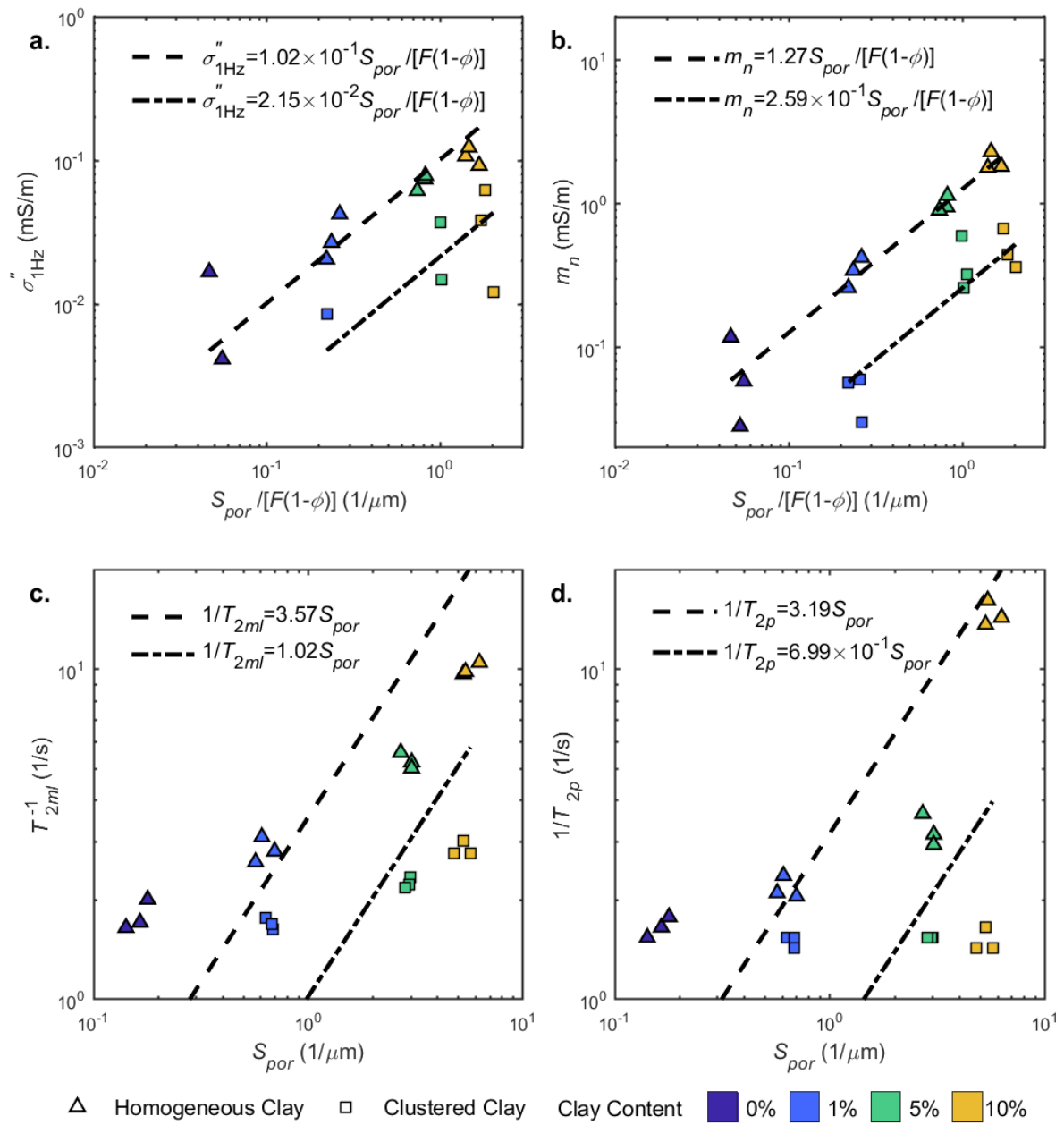
3



1

2 Figure 4

3

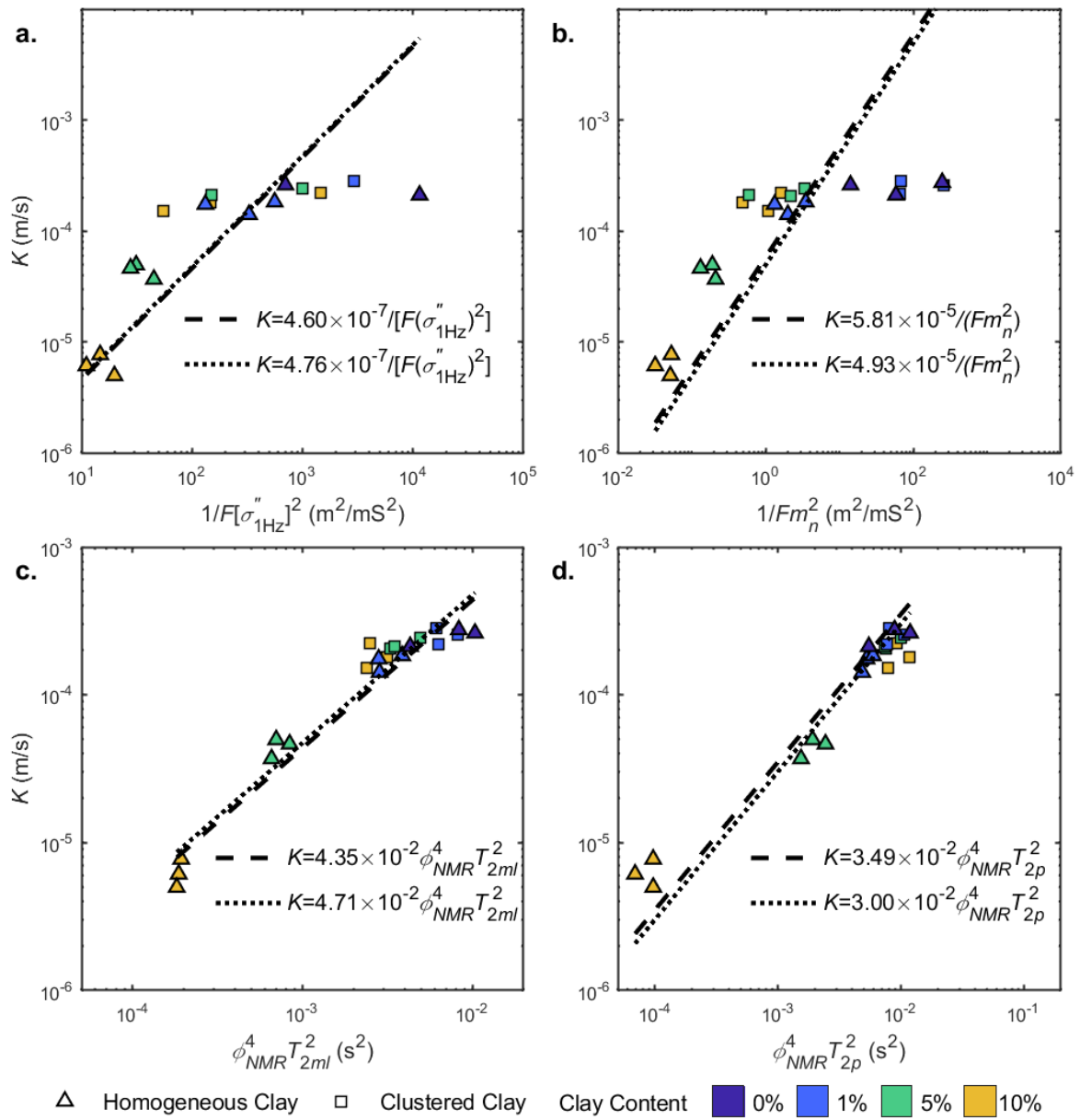


1

2 Figure 5

3

4



1

2 Figure 6